Normal form analysis of bouncing cycles in isotropic rotor stator contact problems

Alexander D. Shaw[a,*], Alan R. Champneys[b], Michael I. Friswell[a]

[a] *College of Engineering, Swansea University, Bay Campus, Fabian Way, Swansea, United Kingdom, SA1 8EN*
[b] *Department of Engineering Mathematics, University of Bristol, Bristol, United Kingdom, BS8 1UB*

Abstract

This work considers analysis of sustained bouncing responses of rotating shafts with nonlinear lateral vibrations due to rotor stator contact. The insight that this is an internal resonance phenomena makes this an ideal system to be studied with the method of normal forms, which assumes that a system may be modelled primarily in terms of just its resonant response components. However, the presence of large non smooth nonlinearities due to impact and rub mean that the method must be extended. This is achieved here by incorporating an alternating frequency/time (AFT) step to capture nonlinear forces. Furthermore, the presence of gyroscopic terms leads to the need to handle complex modal variables, and a rotating coordinate frame must be used to obtain periodic responses. The process results in an elegant formulation that can provide reduced order models of a wide variety of rotor systems, with potentially many nonlinear degrees of freedom. The method is demonstrated by comparing against time simulation of two example rotors, demonstrating high precision on a simple model and approximate precision on a larger model.

1. Introduction

Rotor-stator contact is an issue that affects a wide variety of applications, from turbomachinery [1] to drilling for mineral extraction [2], and is driving a large body of research, see for example [3]. Many rotating devices incorporate magnetic bearing systems [4, 5], and these must be designed with consideration of the consequences of a touch-down event in response to a failure or disturbance [6]. Ehrich [7] has compiled examples of numerous contact phenomena witnessed in tests on turbomachinery, including period-doubling bifurcation routes to chaos, subharmonic resonance and other surprising effects such as bearing phenomenon that lead to a rotor slowly 'switching' between two amplitudes of vibration.

Contact nonlinearities are typically due to friction during contact and discontinuous stiffness effects, and the typical response behaviours are classified by Jacquet-Richardet *et al.* [1] within three classifications; *forward whirl annular motion*, *backward whirl motion*, and *rebounds*. This work is dedicated to the latter of these, which is often the most extreme and certainly the least understood. Rebound motion consists of intermittent contact between rotor and stator, and while many names for forms of this motion are used in the literature (chatter, intermittent contact, rattle, bouncing). We will henceforth refer to these responses as exhibiting *partial contact* motion, or as *bouncing* when brevity is preferred to formality. Some of the earliest work on partial contact motion was summarised in the review by Ehrich [7]. Hallmarks of such motion can be seen in the observation of sum and difference combination resonances in the response of impacting rotors [8], and a case where a nonrigid stator was shown to whirl [9] in a manner apparently similar to a hula-hoop. Neilson and Barr [10] constructed an experimental rig for rotor-stator contact, and showed that the resulting spectral output had synchronous content (i.e. at integer ratios to the drive speed frequency) as well as asynchronous *sidebands*. Many contemporary works continue to

*Corresponding author
Email address: a.d.shaw@swansea.ac.uk (Alexander D. Shaw)

identify and classify the wide variety of phenomena seen due to rotor-stator contact, for example the bifurcation aircraft analysis of a whole engine by Salles *et al.* [11] and the recent experimental work by Ehehalt *et al.* [12].

During the 1980s, researchers began to view these systems through the framework of nonlinear dynamical systems theory [13, 14] and later numerical and experimental studies began to show evidence of period doubling phenomena and chaos. For example Muszynska and Goldman [15] numerically demonstrated bifurcations to period-n motion and transitions to chaos under variation of shaft speed, with good qualitative comparison to experimental results. Chu and Zhang used Floquet analysis of orbits of a contacting Jeffcott rotor to trace the progression to chaos [16]; their results bore similarity to those of [15], where brief regions of chaos where interspersed between wider regions of simpler period-n response. Edwards *et al.* [17] produced a numerical study of a single contacting disk on a shaft, that showed chaotic responses at every integer and half-integer multiples of the first critical drive speed, and demonstrated that this behaviour could be significantly influenced by torsional effects. The review of various nonlinear phenomena by Ishida is also of note [18].

In other work, Karpenko *et al.* developed a piecewise smooth model for rotors experiencing frictionless impacts with a snubber ring [19], and in later work examined the response space of this system with bifurcation analysis, revealing the basins of attraction for various solutions [20]. Pavlovskaia *et al.* [21] considered a similar system, but where the snubber ring springs were preloaded to create additional nonlinearity, and Karpenko *et al.* [22] went on to compare these predictions with experiment , where the experimental stator could rotate on a bearing to approximate the assumption of frictionless contact. Chu and Lu studied a 2-disc experimental system [23], showing some highly complex multi-period and quasiperiodic behaviour, although the authors comment that they could not directly trace the route into chaos due to experimental control issues. Further experimental data has been provided by Torkhani *et al.* on a two disc experimental rig, which also demonstrated agreement with a numerical model [24]. A series of papers by Ishida and Inoue showed analytically and experimentally that 1:(-1) internal resonance between the forward and backward whirls of a nonlinear single disc rotor can drive interesting phenomena, including subharmonic response to out of balance, and reduced critical whirl amplitude [25, 26, 27, 28].

Cole and Keogh [29] emphasise the important distinction between two forms of partial contact motion; *synchronous* partial contact motion that occurs at harmonics and subharmonics of the rotor shaft speed, and *asynchronous* partial contact where the frequency of impacts is apparently unrelated to the shaft speed. That work suggests that synchronous partial contact occurs when the rotor/stator system is anisotropic, a conclusion also supported within the literature cited above. (Typical features that break isotropy are bearings where the vertical stiffness is different to the horizontal stiffness, or a significant gravitational loading on the shaft.) Analysis of asynchronous partial contact motion is harder, because the fundamental frequency of an asynchronous orbit is far less obvious than in the synchronous case. In [29], this frequency was found by balancing the energy immediately before and after an impact accounting for the coefficient of restitution; hence relying on the assumption of instantaneous contact. The same authors use a similar assumption to solve synchronous responses in [30], and it is also interesting to note the recent work of Mora *et al.* [31] who use recent techniques from piecewise-smooth dynamical systems theory to analyse the bifurcations that can occur at primary resonances.

Further insight into asynchronous partial contact motion was demonstrated in the recent paper by Zilli *et al.* [32]. Here they find a condition for isolated bouncing motion of a simple lumped mass rotor that can coexist with the fundamental response curve, well away from any primary resonances. They explained the onset of this motion through a synchronisation condition between the linear forward and backward whirling modes of this system that made it susceptible to asynchronous partial contact motion. This led to an approximate prediction of the drive speeds that could cause this motion. In [33], the present authors reported a generalisation of Zilli's work to multi degree of freedom systems. This showed further forms of asynchronous response, made possible by the increased number of linear whirling modes of the two disk system considered.

Furthermore, it demonstrated that if these responses are viewed in a coordinate system that rotates with the shaft, many of these responses become periodic, and are plainly driven by internal resonance. The works [32, 33] together provided a major step forward in the qualitative understanding of the rich dynamics seen in asynchronous partial contact motion of rotating systems.

The majority of work in this field to date relies on experimental and numerical investigations that are highly time consuming, and it is likely that this has been a barrier to the development of understanding in this field. There is therefore a requirement for improved analytical approaches. Some researchers have employed harmonic balance methods to investigate these systems, seeking the reductions in computation time that these can achieve over numerical time simulation. For example, Kim and Noah [34, 35] found solutions using a method that combined harmonic balance with an alternating frequency time-domain analysis, that assumed two fundamental frequencies, to handle the observed effect that some response frequencies were not periodic in the drive speed frequency. Von Groll and Ewins [36] performed a harmonic balance method on a system where the stator had inertia as well as stiffness, which found both constant contact solutions but also some partial contact solutions. This was augmented with arc-length continuation to trace families of solutions once a solution had been found. Peletan *et al.* again used a harmonic balance procedure augmented with arc-length continuation, but also used the idea of hypertime to allow quasiperiodic solutions, and noted that that method allowed and order of magnitude increase in speed compared to time-marching approaches [37]. For methods to scale to large systems, a form of system reduction is invariably required, and both [34] and [36] use the impedance method to reduce the system to just nonlinear degrees of freedom.

This work presents a new method to find the asynchronous partial contact solutions for isotropic rotors with rotor stator contact nonlinearity, through an adaptation to the method of normal forms. The method of normal forms is a model reduction approach that has been widely applied to nonrotating structures, and works by first applying a modal transformation, and then by reducing the system to just modal frequency components that are resonant using a near-identity transformation [38, 39, 40, 41, 42]. The reduced system is solved by a harmonic balance method, and then approximate information on the non-resonant components is recovered from the transformation, and in this method the non-resonant responses can be used to further refine the solution. This approach is a natural choice given the insight of [33], where it is shown that the responses are dominated by typically just two modes in internal resonance. In principle this remains true even in the presence of large numbers of nonlinear degrees of freedom, meaning that the method should scale well to more complex systems. A further advantage is gained by working in the rotating coordinate system, where quasiperiodic responses become periodic [33], preventing many complications that arise from using two fundamental frequencies for the harmonic balance solution. In order to handle the non-smooth nonlinearities the method incorporates an alternating frequency/time (AFT) step [43, 34], and uses numerical equation-solving to obtain the final results. Furthermore, the method of normal forms is adapted for use on systems with gyroscopic forces and consequent complex underlying linear mode shapes. What results is a compact and elegant general method for dealing with nonlinearity in complex isotropic rotor systems.

The work is organised as follows; Section 2 comprehensively describes the process in a general manner. Then Section 3 details the application to a simple overhung rotor, demonstrating its ability to search for both 2:1 and 3:2 resonant responses. Section 4 then describes the application to a four disc rotor and gives some results for 2:1 internal resonance. Finally, in Section 5 conclusions are presented.

2. Analysis

The normal forms analysis consists of a series of transformations of the equations of motions before a harmonic balance solution can be attempted. An overview of this process is given in Figure 1, and the individual stages are detailed in the

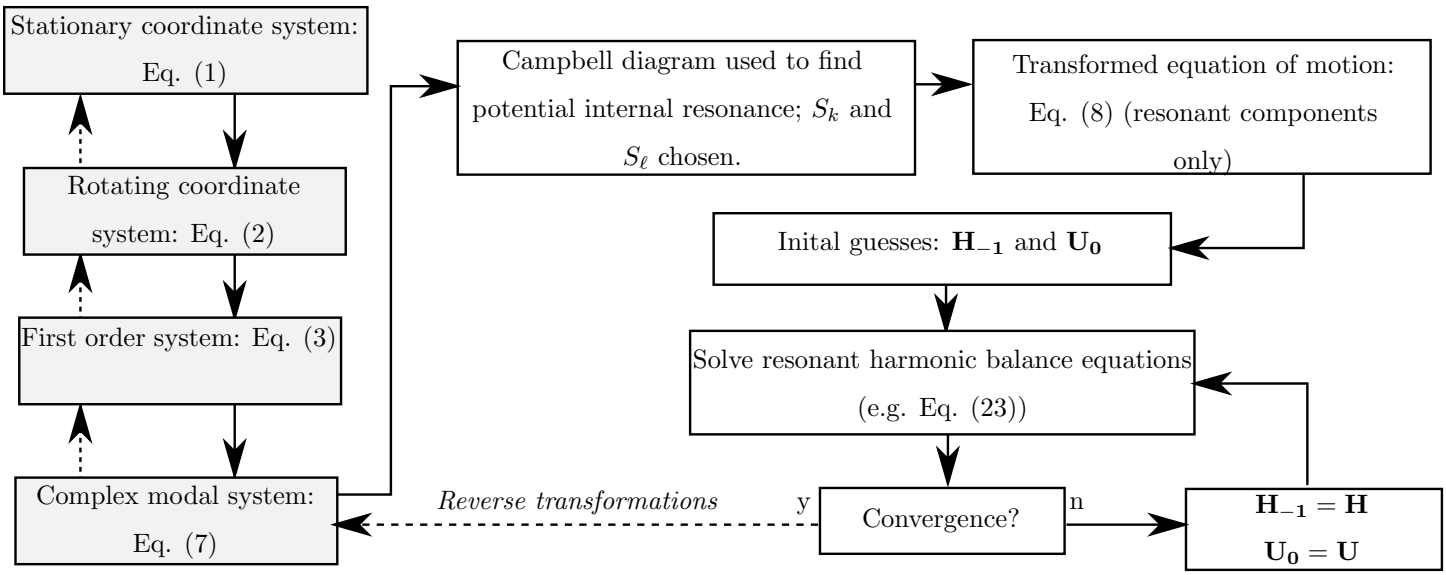

Figure 1: Summary of the normal forms solution process.

following subsections.

2.1. System description

The systems under consideration can be described in terms of models written in the following form in a stationary coordinate system:

$$\mathbf{M}\ddot{\mathbf{x}} + \Omega\bar{\mathbf{G}}\dot{\mathbf{x}} + \bar{\mathbf{K}}\mathbf{x} + \mathbf{C}\dot{\mathbf{x}} + \mathbf{n_x}(\mathbf{x}, \dot{\mathbf{x}}) = \Re\left(\Omega^2\bar{\mathbf{b}}\mathrm{e}^{\jmath\Omega t}\right) \ , \tag{1}$$

where $\mathbf{x} = \mathbf{x}(t)$ is a vector of generalised displacements with size N.[1] Following a time-varying transformation to a coordinate system that rotates with the shaft the transformed equations take the form:

$$\mathbf{M}\ddot{\mathbf{q}} + \Omega\mathbf{G}\dot{\mathbf{q}} + \mathbf{K}\mathbf{q} + \mathbf{C}\dot{\mathbf{q}} + \mathbf{K_c}\mathbf{q} + \mathbf{n_q}(\mathbf{q}, \dot{\mathbf{q}}) = \mathbf{b} \ , \tag{2}$$

where $\mathbf{x} = \mathbf{T}(\Omega t)\mathbf{q}$, with $\mathbf{T}$ a rotation matrix where the rotation angle constantly progresses at the drive speed Ω, which is assumed constant. The square matrices $\mathbf{M}$, $\mathbf{G}$ and $\mathbf{K}$ are the mass, gyroscopic and stiffness matrices respectively. The overbars in equation (1) indicate that $\mathbf{G}$, $\mathbf{K}$ and $\mathbf{b}$ will be different between the two coordinate systems, where the rotating forms will include additional terms that are functions of Ω. The matrix $\mathbf{C}$ is the system linear damping matrix and $\mathbf{K_c}$ contains stiffness-like terms that actually arise due to the transformation of damping forces from the stationary system into the rotating frame. The final term $\mathbf{b}$ represents force due to unbalance; note that this term is constant in time in the rotating coordinate frame. In practice, system matrices are typically generated through finite element methods such as those discussed in [44], or through direct modelling for smaller systems.

2.2. First order form

System (2) is a second order system that cannot be directly diagonalised due to the presence of the first-order term $\Omega\mathbf{G}\dot{\mathbf{q}}$, so therefore it is reduced to first order form as follows:

$$\dot{\mathbf{y}} = \mathbf{A}\mathbf{y} + \mathbf{n_y}(\mathbf{y}) \ , \tag{3}$$

[1] Henceforth (t) is dropped from all state variables and their transformed equivalents for convenience.

where

$$\mathbf{y} = \begin{Bmatrix} \mathbf{q} \\ \dot{\mathbf{q}} \end{Bmatrix}, \quad \mathbf{A} = \begin{bmatrix} \mathbf{0} & \mathbf{I} \\ -\mathbf{M^{-1}K} & -\Omega\mathbf{M^{-1}G} \end{bmatrix}, \quad \mathbf{n_y} = \begin{bmatrix} \mathbf{0} & \mathbf{0} \\ -\mathbf{M^{-1}K_c} & -\Omega\mathbf{M^{-1}C} \end{bmatrix} \mathbf{y} - \begin{Bmatrix} \mathbf{0} \\ \mathbf{n_q(y)} \end{Bmatrix} + \begin{Bmatrix} \mathbf{0} \\ \mathbf{b} \end{Bmatrix},$$

Note that the matrix $\mathbf{A}$ contains the underlying linear conservative system; everything else is bundled into $\mathbf{n_y(y)}$.

2.3. Transformation using undamped complex modes

The eigensolutions of the linear conservative system $\dot{\mathbf{y}} = \mathbf{Ay}$ can be used to transform the system and partly diagonalise system (3). A matrix $\bar{\mathbf{\Phi}}$ is defined, consisting of all eigenvectors of $\mathbf{A}$ placed side by side. Similarly, a diagonal matrix $\bar{\mathbf{\Lambda}}$ contains the eigenvalues of $\mathbf{A}$, to match the ordering of $\bar{\mathbf{\Phi}}$ in the usual way. The transformed system is then given by

$$\dot{\bar{\mathbf{p}}} = \bar{\mathbf{\Lambda}}\bar{\mathbf{p}} + \bar{\mathbf{\Phi}}^{-1}\mathbf{n_y}(\bar{\mathbf{\Phi}}\bar{\mathbf{p}}) \,, \tag{4}$$

where $\mathbf{y} = \bar{\mathbf{\Phi}}\bar{\mathbf{p}}$.

The systems of (3) and (4) have $2N$ states; this seems a little cumbersome when the original system (2) had only N degrees of freedom. Therefore system (4) is reduced by noting that since matrix $\mathbf{A}$ is all real, its eigenvalues and eigenvectors will occur in complex conjugate pairs. The order of modes is chosen such that the modal matrix has the form

$$\bar{\mathbf{\Phi}} = \left[\mathbf{\Phi} \;\middle|\; \mathbf{\Phi}^* \right] \,. \tag{5}$$

Note that the choice of which eigenvector out of a conjugate pair is to be retained in $\mathbf{\Phi}$ is important. An arbitrary choice, such as simply choosing whichever has positive imaginary components, has no physical relevance and will cause the method to fail. The eigenvectors retained in $\mathbf{\Phi}$ are selected by the following procedure:

1. Express the associated eigenvalue in the form $\jmath\tilde{\omega}_{ni}$, and note whether $\tilde{\omega}_{ni}$ is positive or negative
2. Evaluate whether the mode concerned is backward whirling or forward whirling in the rotating coordinate system that is being used, using methods such as those described in [44].
3. If the mode is forward whirling, and $\tilde{\omega}_{ni}$ is positive, retain it. If the mode is backward whirling, and $\tilde{\omega}_{ni}$ is negative, retain it. Otherwise discard it.

This process results in a set of eigenvalues that reflect the physical direction of whirling, in that the value $\tilde{\omega}_{ni}$ can be interpreted as the modal whirling angular velocity in the rotating coordinate system. This also means that they are suitable for the rudimentary arithmetic required in what follows. It is also useful to note that if the equivalent whirling angular velocity in the stationary system is required, it can be found simply by adding the shaft speed:

$$\omega_{ni} = \Omega + \tilde{\omega}_{ni} \,. \tag{6}$$

Note that equation (6) shows that a mode that whirls backward at a small negative whirlspeed such that $0 > \tilde{\omega}_{ni} > -\Omega$ in the rotating system will be seen as having a positive whirlspeed in the stationary system, therefore a slow backward whirl in the rotating systems can appear as a forward whirl in the stationary system. Sorting other matrices to match the retained eigenvectors in $\mathbf{\Phi}$ gives

$$\bar{\mathbf{p}} = \begin{bmatrix} \mathbf{p} \\ \mathbf{p}^* \end{bmatrix}, \quad \bar{\mathbf{\Lambda}} = \left[\begin{array}{c|c} \mathbf{\Lambda} & \mathbf{0} \\ \hline \mathbf{0} & \mathbf{\Lambda}^* \end{array}\right], \quad \bar{\mathbf{\Phi}}^{-1}\mathbf{n_y}(\bar{\mathbf{\Phi}}\bar{\mathbf{p}}) = \begin{bmatrix} \mathbf{n_p(p)} \\ \mathbf{n_p^*(p)} \end{bmatrix},$$

so that finally a system with N complex variables can be extracted from these definitions:

$$\dot{\mathbf{p}} = \mathbf{\Lambda p} + \mathbf{n_p(p)} \,. \tag{7}$$

2.4. Normal form transformation

The method of normal forms seeks a near-identity transformation $\mathbf{p} = \mathbf{u} + \mathbf{h}(\mathbf{u})$ such that the variable $\mathbf{u}$ results in a system

$$\dot{\mathbf{u}} = \mathbf{\Lambda u} + \mathbf{n_u}(\mathbf{u}) \tag{8}$$

that is much simpler equation than (7) to solve. If we subtract (8) from (7) we obtain:

$$\dot{\mathbf{p}} - \dot{\mathbf{u}} = \dot{\mathbf{h}} = \mathbf{\Lambda h} + \mathbf{n_p}(\mathbf{p}) - \mathbf{n_u}(\mathbf{u}) \; . \tag{9}$$

A problem occurs in trying to eliminate $\mathbf{p}$ from this equation in order to solve for $\mathbf{u}$ and $\mathbf{h}$; this has to be done by approximation. At an analytical level, a common approach is to use a Taylor series expansion of $\mathbf{n_p}(\mathbf{p})$. However this is cumbersome in a numerical method. Instead we use a pragmatic predictor-corrector method which improves upon the widely used (for example [39]) approximation $\mathbf{n_p}(\mathbf{u}) = \mathbf{n_p}(\mathbf{p}) + \mathcal{O}(\mathbf{h})$, which works well in systems where $\mathbf{h}$ contains only very small components. It shall be seen that in these cases, $\mathbf{h}$ can become larger due to constant (or synchronous) terms that can have an important symmetry-breaking effect [45]. Specifically, we assume that

$$\mathbf{n_p}(\mathbf{p}) \approx \mathbf{n_p}(\mathbf{u} + \mathbf{h_{-1}}) = \mathbf{n_p}(\mathbf{p_{-1}}) \; , \tag{10}$$

with accuracy of $\mathcal{O}(\mathbf{h_0} - \mathbf{h_{-1}})$ where $\mathbf{h_{-1}}$ is an estimate from a previous iteration or initial guess $\mathbf{h}$, and $\mathbf{h_0}$ is the true value for $\mathbf{h}$. Of course, this raises the problem of choosing a suitable initial guess for $\mathbf{h_{-1}}$ to get the process started. However, it has been found that in general the underlying damped linear out-of-balance solution is a reasonable choice. After incorporating this approximation, equation (9) can be rearranged to:

$$\dot{\mathbf{h}} - \mathbf{\Lambda h} - \mathbf{n_p}(\mathbf{u} + \mathbf{h_{-1}}) + \mathbf{n_u}(\mathbf{u}) = \mathbf{0} \; . \tag{11}$$

Note that the actual form of the transformation $\mathbf{h}(\mathbf{u})$ will be determined in the frequency domain along with the trial solution, which we describe in the next section.

2.5. Trial solution in frequency domain using a matrix representation

The general solution of $\mathbf{u}$ can be written in the frequency domain as

$$\mathbf{u} = \sum_{\ell=-n_f/2}^{n_f/2-1} \mathbf{U}_\ell \mathrm{e}^{\ell \jmath \omega_r t} = \mathbf{U t} \; , \tag{12}$$

i.e. a summation of vectors multiplied by exponential time functions, so that each transformed modal variable is represented by a complex Fourier series with unknown fundamental frequency ω_r and signed harmonics. In the matrix form $\mathbf{Ut}$, $\mathbf{U}$ will have dimensions $N \times n_f$ where n_f indicates the length of the Fourier series, and the harmonic vector $\mathbf{t}$ will be a vector of all the terms $\mathrm{e}^{\ell \jmath \omega_r t}$ with length n_f. Note that we have assumed that n_f is even. The aim is a system where $\mathbf{u}$ is simple, and therefore it is desirable that $\mathbf{U}$ is as sparse as possible. Similar representations are made for all other variables:

$$\mathbf{h} = \mathbf{H t} \; , \; \mathbf{n_u}(\mathbf{u}) = \mathbf{N_u t} \; , \; \mathbf{n_p}(\mathbf{u} + \mathbf{h_{-1}}) = \mathbf{N_p t} \; , \; \mathbf{h_{-1}} = \mathbf{H_{-1} t} \; , \; \mathbf{p_{-1}} = \mathbf{P_{-1} t} \; . \tag{13}$$

In principle these forms have accuracy limited by approximation (10) and by the number of points in the Fourier series, n_f. As shall be seen, for larger systems it will usually be necessary to limit the number of modes retained in Φ, and also higher harmonics may have to be zeroed, further limiting accuracy. Differentiation can also be achieved by noting that

$$\dot{\mathbf{h}} = \mathbf{H}\dot{\mathbf{t}} = \mathbf{H \Psi t} \; , \tag{14}$$

where $\mathbf{\Psi}$ is an $n_f \times n_f$ diagonal matrix where the ℓth diagonal entry has form $\Psi_{\ell,\ell} = \ell\jmath\omega_r$. Furthermore, a shorthand is henceforth applied to indexing matrix elements which refer to signed Fourier components; the ℓth row or column actually refers to whichever row or column relates to the ℓth harmonic. This saves having to constantly refer to a mapping between a signed harmonic and a positive integer matrix index[2].

Thus equation (11) may be written:

$$\mathbf{H\Psi t} - \mathbf{\Lambda H t} - \mathbf{N_p t} + \mathbf{N_u t} = \mathbf{0} \; . \tag{15}$$

2.6. Evaluating the modal nonlinear function matrix $\mathbf{N_p}$

In order to evaluate the trial nonlinear frequency components an alternating frequency/time (AFT) step is used. This consists of

1. Evaluating the trial solution in the time domain.
2. Evaluating all nonlinear and nonconservative forces based on this time series.
3. Using a Fast Fourier Transform (FFT) to return the frequency components of the forces.

Firstly, the time series of $\mathbf{p_{-1}}$ used in approximation (10) is expressed using the forms in (13):

$$\mathbf{p_{-1}} = (\mathbf{U} + \mathbf{H_{-1}})\,\mathbf{t} \; . \tag{16}$$

Equation (16) is evaluated at each time step of the period $t_i = \frac{2\pi}{n_f \omega_r}[1, 2...n_f]$ using an inverse complex FFT $\mathbf{f}(..)$:

$$\mathbf{p_{-1}}_i = \mathbf{f}\left(\mathbf{U} + \mathbf{H_{-1}}\right) \; . \tag{17}$$

Note that the value of any $\mathbf{p_{-1}}_i$ does not vary with ω_r, so an arbitrary value for the fundamental ω_r can be used for evaluation of this stage (the true value of ω_r is an unknown that must be solved). Note that $\mathbf{U}$ is sought to be sparse, whereas $\mathbf{H_{-1}}$ is a matrix of constants from a previous solution or initial guess, and is in general full except for elements where $\mathbf{U}$ is nonzero.

Now the discrete time series of approximation (10) can be evaluated using the complex modally transformed nonlinear/nonconservative function $\mathbf{n_p}(...)$:

$$\mathbf{n_p}_i = \mathbf{n_p}(\mathbf{p_{-1}}_i) \; . \tag{18}$$

It is then straightforward to get the Fourier components using a complex FFT $\mathbf{F}(...)$:

$$\mathbf{N_p} = \mathbf{F}(\mathbf{n_p}_i) \; . \tag{19}$$

2.7. Choosing the transformation matrices $\mathbf{H}$ *and* $\mathbf{N_u}$

Note that corresponding elements k, ℓ of the matrices in (15) can be compared separately because they each relate to a different harmonic of a different modal variable. Hence equation (15) (with $\mathbf{t}$ eliminated) can be considered term by term:

$$H_{k,\ell}\Psi_{\ell,\ell} - \Lambda_{k,k}H_{k,\ell} - N_{p(k,\ell)} + N_{u(k,\ell)} = 0 \; , \tag{20}$$

where the convention for ℓ used in (14) is used. In general, because we want to simplify equation (8), equation (20) is solved by choosing

$$N_{u(k,\ell)} = 0 \; , \qquad H_{k,\ell} = \frac{N_{p(k,\ell)}}{\Psi_{\ell,\ell} - \Lambda_{k,k}} \; . \tag{21}$$

[2]Many implementations of the complex FFT for even n_f return an array with the positive harmonics from 0 to $n_f/2 - 1$ appear consecutively in positions 1 to $n_f/2$, followed by negative harmonics from $-n_f/2$ to -1 appearing in positions $n_f/2+1$ to n_f. This mapping can be conveniently expressed by the mapping from signed harmonic ℓ to matrix index i as $\ell \to i = 1 + \ell \mod n_f$, and the reverse mapping $i \to \ell = i - 1 - n_f \lfloor \frac{2(i-1)}{n_f} \rfloor$.

However, if $\Psi_{\ell,\ell} \approx \Lambda_{k,k}$, this will cause $H_{k,\ell}$ to be large, violating the assumption of a near identity transformation. These components are known as resonant terms [46] and must be solved by choosing:

$$N_{u(k,\ell)} = N_{p(k,\ell)} \ , \qquad H_{k,\ell} = 0 \ , \tag{22}$$

and then solving as part of the frequency domain solution to equation (8). Note that while (21) can be used to 'test' terms for resonance, in practice the form of anticipated internal resonance is chosen prior to attempting the solution, based on consideration of the underlying system in a similar manner to [33]. This process is formalised by the definition of two ordered lists, S_k and S_ℓ, which contain the numbers of the modes involved in resonance, and their harmonics of the fundamental frequency respectively. Examples of how to define these will be given in Section 3.4 and in Section 4.2.

2.8. Solving the resonant equation

Typically interesting solutions (i.e. not simply synchronous whirling in or out of contact) occur when exactly two modes become internally resonant [33], hence (8) will reduce to a harmonic balance problem of the form:

$$\begin{aligned} U_{i,j}\Psi_{j,j} - \Lambda_{i,i}U_{i,j} - N_{u(i,j)} = 0 \\ U_{k,\ell}\Psi_{\ell,\ell} - \Lambda_{k,k}U_{k,\ell} - N_{u(k,\ell)} = 0 \end{aligned} \ . \tag{23}$$

Hence our system of N degrees of freedom has been reduced to the form of two complex equations. Equation (23) has 5 unknowns; the real and imaginary parts of $U_{i,j}$ and $U_{k,\ell}$ and also the unknown fundamental frequency ω_r which is appears in $\Psi_{j,j}$ and $\Psi_{\ell,\ell}$ (see the definition of $\mathbf{\Psi}$ following eqn. (14)). However, we may impose that one of the transformed modal variables is either purely real or purely imaginary; this constrains the phase of this modal variable and therefore locks the phase of the solution. Therefore, with this imposition equation is (23) is solvable.

It is clearly possible to rearrange (23) into the form

$$\mathbf{g}_{4\times1}(\mathbf{U}^*, \omega_r) = 0 \ ,$$

where $\mathbf{U}^*$ is a 3×1 vector of all the unknown (and nonzero) parts of $U_{i,j}$ and $U_{k,\ell}$, and then solve it with any nonlinear equation solving algorithm. However, it is possible to further assist the solving algorithm by noting that each row of equation (23) is linear in ω_r ; therefore ω_r can always be directly obtained from one real or imaginary component of one of the equations. For example, the imaginary part of the second line of equation (23) could be solved by exploiting the form of the various matrices to find

$$\omega_r = \frac{\Re\left(U_{k,\ell}\right)\tilde{\omega}_{nk} + \Im\left(N_{u(k,\ell)}\right)}{\ell\Re\left(U_{k,\ell}\right)} \ . \tag{24}$$

Hence, the smaller system

$$\mathbf{g}_{3\times1}(\mathbf{U}^*) = 0 \ , \tag{25}$$

can be solved instead, where this linear stage for ω_r is incorporated into the definition of $\mathbf{g}_{3\times1}(...)$.

3. Example 1 - A snubbed overhung rotor

3.1. General description

The system considered is similar to that proposed by Zilli in [32]; however a different notation is used and alternative forms for the nonlinearity are considered. The system is as depicted in figure 2 (a). A disc of mass m, polar moment of inertia I_p, and diametral moment inertia I_d, is mounted on an inertialess rigid shaft of length ℓ. The shaft is pinned at point O, and

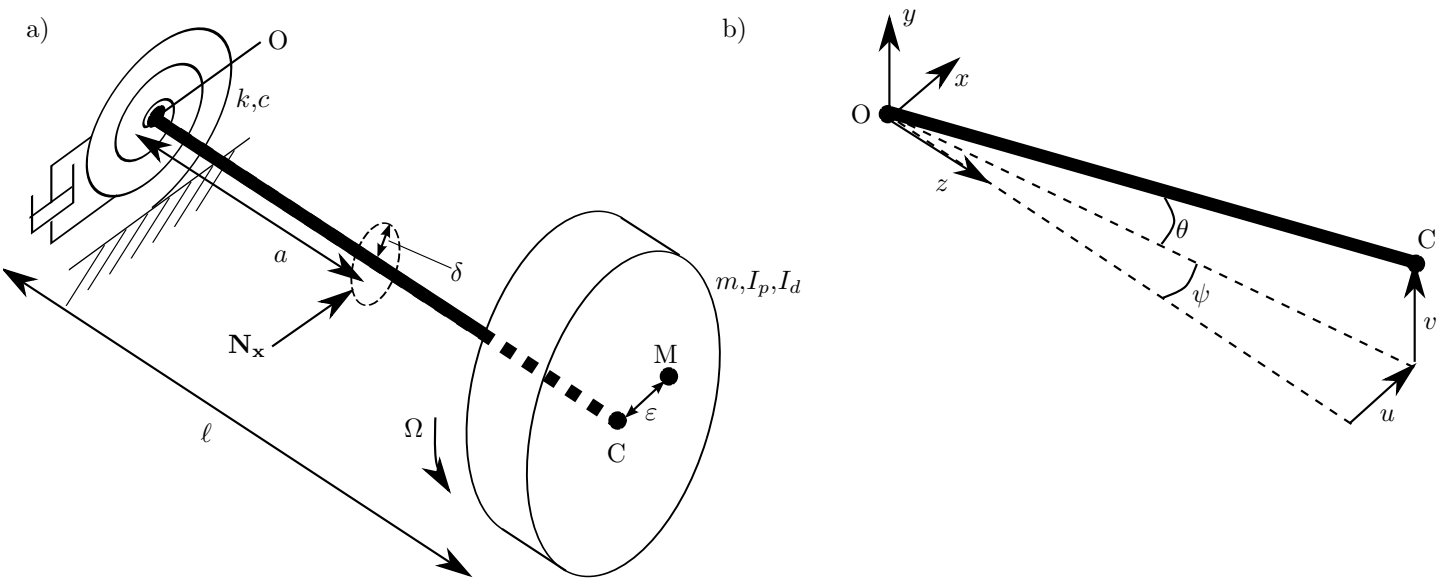

Figure 2: a) A snubbed overhung rotor. b) Assumed kinematics of point C.

rotations around this point are resisted by a linear isotropic rotational viscously damped spring, with rate k and damping coefficient c. The disc rotates at a constant angular speed Ω about its centre point C; however imperfections in its geometry cause its centre of mass M to be at a distance ε from C, resulting in out of balance forces. A stator with clearance δ exists at a distance a along the shaft. This generates additional restoring forces when the displacement at this point is greater than δ, represented by the nonlinear contact force $\mathbf{N_x}$.

The disc will exhibit coupled translational and rotational responses; Figure 2 (b) shows that angular and translational displacements are coupled by

$$u = \psi\ell \ , \ v = -\theta\ell \ , \tag{26}$$

where the sign of rotations has been determined by the right-hand screw convention, and ψ and θ are assumed to remain small to allow linearising assumptions. Furthermore, Figure 2 shows that contact will occur when

$$\sqrt{u^2 + v^2} > \Delta \ , \ \Delta = \frac{\delta\ell}{a} \ . \tag{27}$$

Using equation (26), all kinetic and potential energy can be evaluated in terms of the chosen displacement variables, and Lagrangian mechanics can therefore be used to derive the following equations of motion:

$$\begin{aligned} M\ddot{u} + \frac{I_p}{\ell^2}\Omega\dot{v} + \frac{k}{\ell^2}u + \frac{c}{\ell^2}\dot{u} &= m\varepsilon\Omega^2\cos\Omega t + N_u(u, v, \dot{u}, \dot{v}) \ , \\ M\ddot{v} - \frac{I_p}{\ell^2}\Omega\dot{u} + \frac{k}{\ell^2}v + \frac{c}{\ell^2}\dot{v} &= m\varepsilon\Omega^2\sin\Omega t + N_v(u, v, \dot{u}, \dot{v}) \ , \end{aligned} \tag{28}$$

where $N_u(u, v, \dot{u}, \dot{v})$ and $N_v(u, v, \dot{u}, \dot{v})$ are the components of $\mathbf{N_x}$ in the u and v directions respectively, and $M = m + \frac{I_d}{\ell^2}$.

3.2. Nondimensionalisation

Time is nondimensionalised by the undamped natural frequency of the underlying nonrotating system:

$$\tau = \omega_n t \ , \ \omega_n = \sqrt{\frac{k}{M\ell^2}} \ , \tag{29}$$

and henceforth differentiation with respect to τ shall be denoted by a prime ($'$). Displacements are nondimensionalised by the displacement magnitude required for contact:

$$\hat{u} = \frac{u}{\Delta} \ , \ \hat{v} = \frac{v}{\Delta} \ . \tag{30}$$

Furthermore, the following definitions are made to scale the polar moment of inertia, driving frequency, out of balance forcing and damping:

$$\hat{I}_p = \frac{I_p}{M\ell^2} \quad , \quad \hat{\Omega} = \frac{\Omega}{\omega_n} \quad , \quad \hat{f} = \frac{m\varepsilon}{M\Delta} \quad , \quad \zeta = \frac{c}{2\ell^2\omega_n M} \, , \tag{31}$$

and the nonlinear contact forces are also scaled accordingly:

$$\begin{aligned} \hat{N}_u\left(\hat{u},\hat{v},\hat{u}',\hat{v}'\right) &= \frac{1}{\Delta\omega_n^2 M} N_u\left(\Delta\hat{u},\Delta\hat{v},\omega_n\Delta\hat{u}',\omega_n\Delta\hat{v}'\right) \\ \hat{N}_v\left(\hat{u},\hat{v},\hat{u}',\hat{v}'\right) &= \frac{1}{\Delta\omega_n^2 M} N_v\left(\Delta\hat{u},\Delta\hat{v},\omega_n\Delta\hat{u}',\omega_n\Delta\hat{v}'\right) \, , \end{aligned} \tag{32}$$

Substituting equations (29) to (32) into equation (28) gives the nondimensional equations of motion:

$$\begin{aligned} \hat{u}'' + \hat{I}_p\hat{v}' + \hat{u} + 2\zeta\hat{u}' &= \hat{f}\hat{\Omega}^2\cos\hat{\Omega}\tau + \hat{N}_u\left(\hat{u},\hat{v},\hat{u}',\hat{v}'\right) \\ \hat{v}'' - \hat{I}_p\hat{u}' + \hat{v} + 2\zeta\hat{v}' &= \hat{f}\hat{\Omega}^2\sin\hat{\Omega}\tau + \hat{N}_v\left(\hat{u},\hat{v},\hat{u}',\hat{v}'\right) \, , \end{aligned} \tag{33}$$

If we define $\mathbf{x} = \{\hat{u},\hat{v}\}^T$ this can be expressed in matrix form as

$$\mathbf{x}'' + \begin{bmatrix} 0 & \hat{I}_p \\ -\hat{I}_p & 0 \end{bmatrix}\mathbf{x}' + \mathbf{x} + 2\zeta\mathbf{x}' = \hat{f}\hat{\Omega}^2\begin{bmatrix}\cos\hat{\Omega}\tau \\ \sin\hat{\Omega}\tau\end{bmatrix} + \mathbf{N}_\mathbf{x}\left(\mathbf{x},\mathbf{x}'\right) \, , \tag{34}$$

which is clearly in the form of equation (1).

3.3. Transformation to rotating coordinate system

The transformation between the rotating coordinates and the stationary coordinates is defined in matrix form as

$$\mathbf{x} = \begin{Bmatrix}\hat{u}\\ \hat{v}\end{Bmatrix} = \begin{bmatrix}\cos\hat{\Omega}\tau & -\sin\hat{\Omega}\tau \\ \sin\hat{\Omega}\tau & \cos\hat{\Omega}\tau\end{bmatrix}\begin{Bmatrix}\tilde{u}\\ \tilde{v}\end{Bmatrix} = \mathbf{T}\mathbf{q} \, , \tag{35}$$

Equation (33) can be transformed to the rotating system by substituting equation (35) and premultiplying by $\mathbf{T}^{-1} = \mathbf{T}^T$, applying the chain rule as necessary. Using the identities $\mathbf{T}^T\mathbf{T}' = \hat{\Omega}\mathbf{J}$, where $\mathbf{J} = \begin{bmatrix}0 & -1\\ 1 & 0\end{bmatrix}$, and $\mathbf{T}'' = -\hat{\Omega}^2\mathbf{T}$ leads to the nondimensional equation of motion in the rotating coordinate system:

$$\mathbf{q}'' - \hat{\Omega}(\hat{I}_p - 2)\mathbf{J}\mathbf{q}' + (1 - \hat{\Omega}^2(1-\hat{I}_p))\mathbf{q} - 2\zeta\hat{\Omega}\mathbf{J}\mathbf{q} + 2\zeta\mathbf{q}' = \begin{Bmatrix}\hat{f}\hat{\Omega}^2\\ 0\end{Bmatrix} + \mathbf{N}_\mathbf{q}(\mathbf{q},\mathbf{q}') \, . \tag{36}$$

This is in the form of system (2) with matrices as follows:

$$\begin{gathered} \mathbf{M} = \mathbf{I}_{2\times2} \, , \; \mathbf{G} = -(\hat{I}_p - 2)\mathbf{J} \, , \; \mathbf{K} = (1 - \hat{\Omega}^2(1-\hat{I}_p))\mathbf{I}_{2\times2} \, , \; \mathbf{C} = 2\zeta\mathbf{I}_{2\times2} \\ \mathbf{K_c} = -2\zeta\hat{\Omega}\mathbf{J} \, , \; \mathbf{b} = \left\{\hat{f}\hat{\Omega}^2, 0\right\}^T \end{gathered} \, ,$$

and it is assumed that the nonlinear contact function is isotropic hence

$$\mathbf{N}_\mathbf{q}\left(\mathbf{q},\dot{\mathbf{q}}\right) = \mathbf{N}_\mathbf{x}\left(\mathbf{q},\dot{\mathbf{q}} + \hat{\Omega}\mathbf{J}\mathbf{q}\right) \, , \tag{37}$$

where the term $\hat{\Omega}\mathbf{J}\mathbf{q}$ will only have any effect if the nonlinearity contains tangential velocity components e.g. friction. In this example we shall consider purely radial stiffness and damping i.e.

$$\mathbf{N}_\mathbf{q}\left(\mathbf{q},\dot{\mathbf{q}}\right) = \begin{cases} \left(\hat{k}_s(r-1) + \hat{c}_s r'\right)\mathbf{q}/r \, , & \text{if } r \geq 1 \\ \mathbf{0} \, , & \text{if } r < 1 \end{cases} \, , \tag{38}$$

where $\hat{k}_s$ and $\hat{c}_s$ are nondimensional stator stiffness and damping respectively and $r = |\mathbf{q}|$.

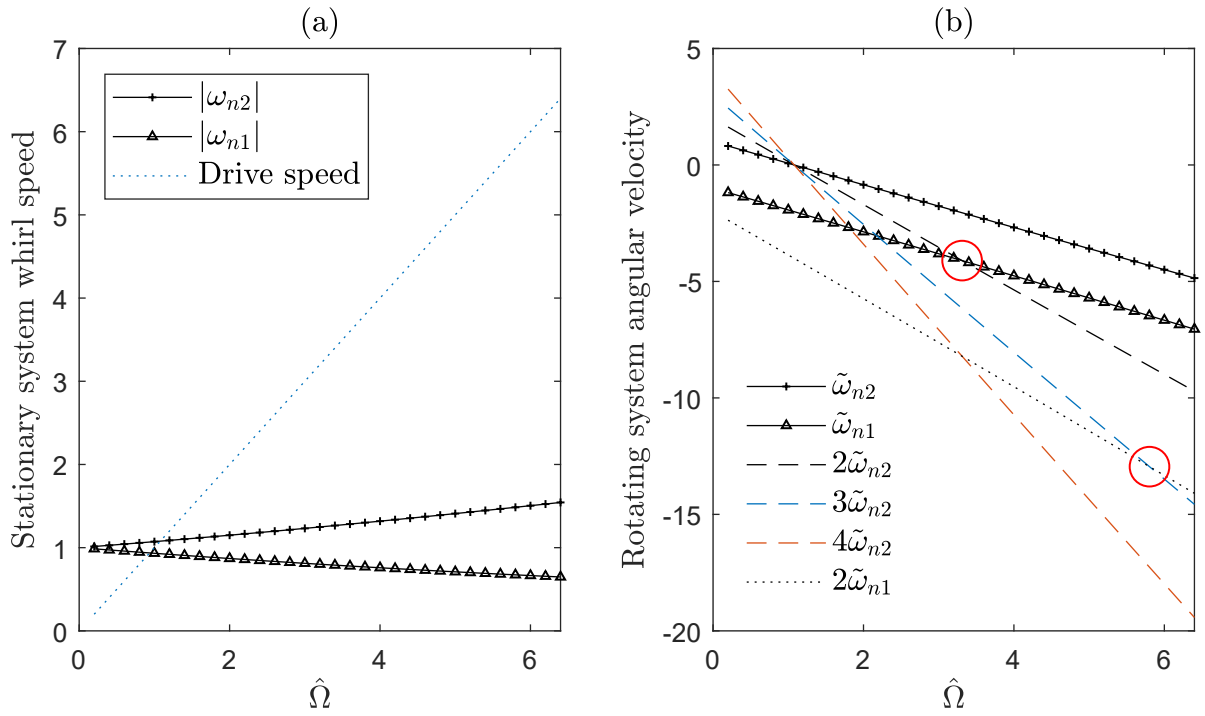

Figure 3: (a) Campbell diagram showing nondimensional undamped backward ($|\omega_{n1}|$) and forward ($|\omega_{n2}|$) whirl *speeds* in stationary coordinate frame, $\hat{I}_p = 0.14$. (b) Equivalent angular *velocities* in the rotating frame, plus selected integer multiples. Circles highlight the nonlinear critical speeds for 2:1 and 3:2 internal resonance.

3.4. Solution

The steps of sections 2.2 and 2.3 are applied to (36). The two eigensolutions of $\mathbf{A}$ relate to the well-known backward and forward whirl modes of an overhung rotor. The whirl velocities relating to the backward whirl mode are labelled ω_{n1} and $\tilde{\omega}_{n1}$ in the stationary and rotating frames respectively. Similarly the whirl velocities relating to the forward whirl mode are labelled ω_{n2} and $\tilde{\omega}_{n2}$. The eigenvector matrix is

$$\mathbf{\Phi} = \begin{bmatrix} 1, 1 \\ -\jmath, -\jmath \end{bmatrix} . \tag{39}$$

The above eigenanalysis and (6) can be used over a range of drive speeds to produce the traditional Campbell diagram shown in Figure 3 (a), showing the unsigned whirl speeds in the stationary frame; this is the classic representation of natural frequencies of a rotating system [44]. However a more useful diagram in this case is shown in Figure 3 (b), which shows signed angular velocities in the rotating frame. The sign of these velocities indicate whether the motion is forward whirling (i.e anticlockwise, same direction as the shaft rotation) or backward whirling (i.e. clockwise, opposite to the shaft rotation). Figure 3 (b) also includes some lines to indicate integer multiples of these velocities.

To begin the normal form transformation process, there must be some initial assumptions about the expected form of internal resonance and roughly at what drive speeds these may occur. Figure 3 (b) shows that at $\hat{\Omega} \approx 3.3$ there is a 2:1 ratio between $\tilde{\omega}_{n2}$ and $\tilde{\omega}_{n1}$. Following [32] and [33], asynchronous partial contact cycles are found numerically at drive speeds just above this point, so this drive speed will be used to begin searching for 2:1 resonance motion. Hereupon, we will introduce the term *nonlinear critical speed* to refer to a condition such as this; specifically the drive speed $\hat{\Omega} \approx 3.3$ is the nonlinear critical speed for 2:1 resonance. It may be seen from Figure 3 (b) that many nonlinear critical speeds exist for even a simple rotor such as this; in particular the nonlinear critical speed for 3:2 internal resonance at $\hat{\Omega} \approx 5.8$ is also highlighted.

To formalise our assumption about internal resonance, two ordered lists are created to state which modes and harmonics

are considered resonant. Firstly, S_k is the list of modes involved in the solution - for this simple system this is trivial, $S_k = 1, 2$ because there are only two underlying linear modes. The second list defines the signed nonlinear resonant response frequency for each mode, as a harmonic of the positive fundamental response frequency ω_r, and is denoted S_ℓ. This can be determined graphically, with reference to Figure 3 (b). For example, for the 2:1 resonance, we see that at the relevant nonlinear critical speed, both $\tilde{\omega}_{n1}$ and $\tilde{\omega}_{n2}$ are negative, so we choose $S_\ell = -2, -1$ (respecting the order of S_k). The physical interpretation of this is that in the vicinity of the relevant nonlinear critical speed in Figure 3 (b), we are anticipating an internally resonant orbit where the first modal variable is mainly responding at an angular velocity of $-1\omega_r$, and the second modal variable is mainly responding at an angular velocity of $-2\omega_r$. Furthermore, both of these response velocities are similar to their respective underlying linear modal angular velocities. Similarly, for the 3:2 case $S_\ell = -3, -2$, because mode 1 will be resonant at a frequency of $-3\omega_r$ and mode 2 at a frequency of $-2\omega_r$.

A harmonic balance equation of the form

$$U_{k,\ell}\Psi_{\ell,\ell} - \Lambda_{k,k}U_{k,\ell} - N_{u(k,\ell)} = 0 \ , \tag{40}$$

can then be defined for each k in S_k with the respective ℓ from S_ℓ. Hence for the 2:1 case the resonant harmonic balance equations in the form of (23) are

$$\begin{aligned} U_{1,-2}\Psi_{-2,-2} - \Lambda_{1,1}U_{1,-2} - N_{u(1,-2)} = 0 = -2\jmath\omega_r U_{1,-2} - \jmath\tilde{\omega}_{n1}U_{1,-2} - N_{u(1,-2)} \ , \\ U_{2,-1}\Psi_{-1,-1} - \Lambda_{2,2}U_{2,-1} - N_{u(2,-1)} = 0 = -\jmath\omega_r U_{2,-1} - \jmath\tilde{\omega}_{n2}U_{2,-1} - N_{u(2,-1)} \ , \end{aligned} \tag{41}$$

where the right-hand side shows $\mathbf{\Lambda}$ and $\mathbf{\Psi}$ expanded to reveal the presence of ω_r and $\tilde{\omega}_{nk}$ in the equations. Similarly, the following resonant harmonic balance equations are found for the 3:2 resonance

$$\begin{aligned} U_{1,-3}\Psi_{-3,-3} - \Lambda_{1,1}U_{1,-3} - N_{u(1,-3)} = 0 = -3\jmath\omega_r U_{1,-3} - \jmath\tilde{\omega}_{n1}U_{1,-3} - N_{u(1,-3)} \ , \\ U_{2,-2}\Psi_{-2,-2} - \Lambda_{2,2}U_{2,-2} - N_{u(2,-2)} = 0 = -2\jmath\omega_r U_{2,-2} - \jmath\tilde{\omega}_{n2}U_{2,-2} - N_{u(2,-2)} \ . \end{aligned} \tag{42}$$

The final step before attempting to solve the above equations is an initial guess for $\mathbf{H_{-1}}$, as required by approximation (10). It emerges that the linear synchronous whirling response, with solutions in many texts e.g [44], generally gives good results once the relevant transformations have been applied. This is fortunate, because it means that the only starting guesses that need to be made before solving are for the resonant components.

With all this initial transformation work done, we are finally in a position to attempt a solution. We define a target function that will allow us to numerically solve the resonant equation (23) using an AFT process. This function takes $\mathbf{U}$ as an input and performs the following steps:

1. Add the current estimate of $\mathbf{U}$ to $\mathbf{H_{-1}}$ to form $\mathbf{P_{-1}}$, an approximation of $\mathbf{P}$.
2. Use an inverse complex Fourier transform to obtain the time sequence of $\mathbf{p_{-1}}_i$ for $i = 1...n_f$.
3. Evaluate the time series of nonlinear and nonconservative force $\mathbf{n_p}_i$, by applying equation (18) at each time step.
4. Using a complex Fourier transform to obtain $\mathbf{N_p}$ from $\mathbf{n_p}_i$.
5. Evaluate $\mathbf{N_u}$ - zero everywhere except for components deemed resonant through choice of S_k and S_ℓ.
6. Solve for ω_r with something in the form of eqn. (24), and use this to evaluate $\mathbf{\Psi}$.
7. For each k and ℓ in S_k and S_ℓ respectively evaluate $U_{k,\ell}\Psi_{\ell,\ell} - \Lambda_{k,k}U_{k,\ell} - N_{u(k,\ell)}$ and append the real and imaginary components to the residual vector.

A numerical solver is used to find roots of the above target function, giving the next estimate for $\mathbf{U}$.

Once $\mathbf{U}$ has been found, a corresponding value for $\mathbf{H}$ can be calculated with equation (21). This value may be passed into $\mathbf{H_{-1}}$, and the whole process iterated until $\mathbf{H} = \mathbf{H_{-1}}$, following the process in Figure 1. When the accuracy is sufficient,

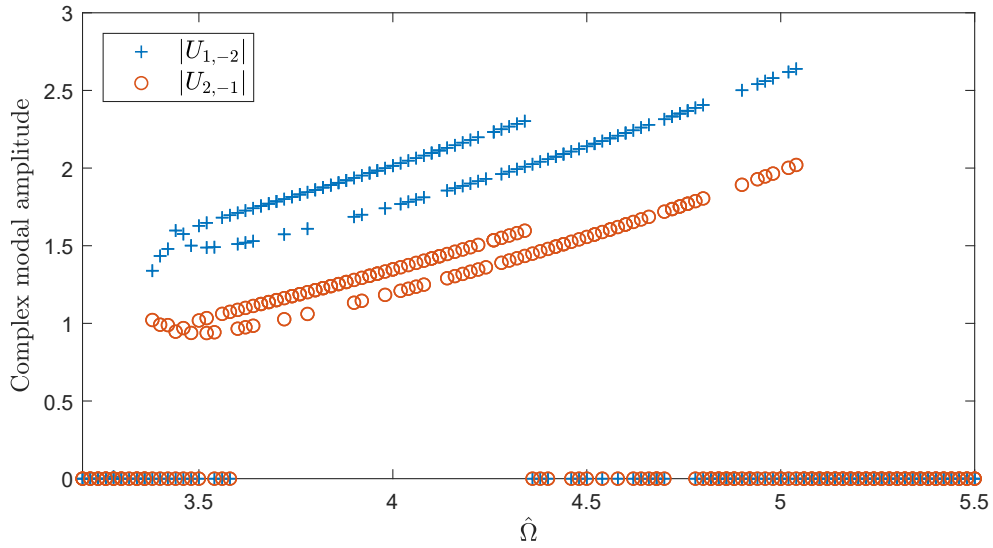

Figure 4: Complex modal amplitudes of resonant components of responses with 2:1 internal resonance at various drive speeds.

$\mathbf{P}$ can be evaluated, then the entire result transformed back to the time domain with an inverse complex FFT. Then the modal variables can be transformed back to spatial variables using

$$\mathbf{y} = \bar{\mathbf{\Phi}}\bar{\mathbf{p}} = \mathbf{\Phi}\mathbf{p} + \mathbf{\Phi}^*\mathbf{p}^* = 2\Re\left(\mathbf{\Phi}\mathbf{p}\right) \tag{43}$$

and physical reflections can be made.

3.5. Results

The following results are for a system with the following parameters; $\hat{I}_p = 0.14$, $\zeta = 0.01$, $\hat{f} = 0.0648$, $\hat{k}_s = 13.2$, $\hat{c}_s = 0.0232$. The number of points in the FFT is $n_f = 1024$; note that for relatively weak nonlinearity much lower values for n_f may be used and still give acceptable results, although care must be taken to avoid the possibility of aliasing.

The value of $\mathbf{H}_{-1}$ is taken to be the linear synchronous whirl solution on the initial run; the solution is then iterated two more times to improve accuracy. Four trial starting values for $\mathbf{U}$ were used which were all permutations of:

$$\begin{gathered} U_{1,-2} = 1.5 \\ U_{2,-1} = -1.5,\ -1.5\jmath,\ 1.5,\ 1.5\jmath \\ \text{all other } U_{k,\ell} = 0, \text{ as these are not resonant.} \end{gathered} \tag{44}$$

These were chosen to give reasonable penetration into the stator, and to give a range of phases for $U_{2,-1}$.

3.5.1. 2:1 resonance

Figure 4 shows results of this process, in terms of the resonant components $U_{1,-2}$ and $U_{2,-1}$, over a range of shaft speeds. As may be seen, in many cases both resonant components are zero. This indicates a simple synchronous whirling motion, which for the purpose of this investigation is considered trivial. At $\hat{\Omega} = 3.38$, the first non-trivial solution appears. Note that this is slightly above the nonlinear critical speed given by Figure 3, in keeping with numerical observations in [33, 32]. For higher shaft speeds, after some noisy looking points, two rows of solutions for each component appear, and this situation persists up to approximately $\hat{\Omega} = 4.48$. The higher amplitude responses for $|U_{1,-2}|$ correspond to the higher amplitude responses for $|U_{2,-1}|$, and similarly the lower amplitude responses for $|U_{1,-2}|$ correspond to the lower amplitude responses for $|U_{2,-1}|$.

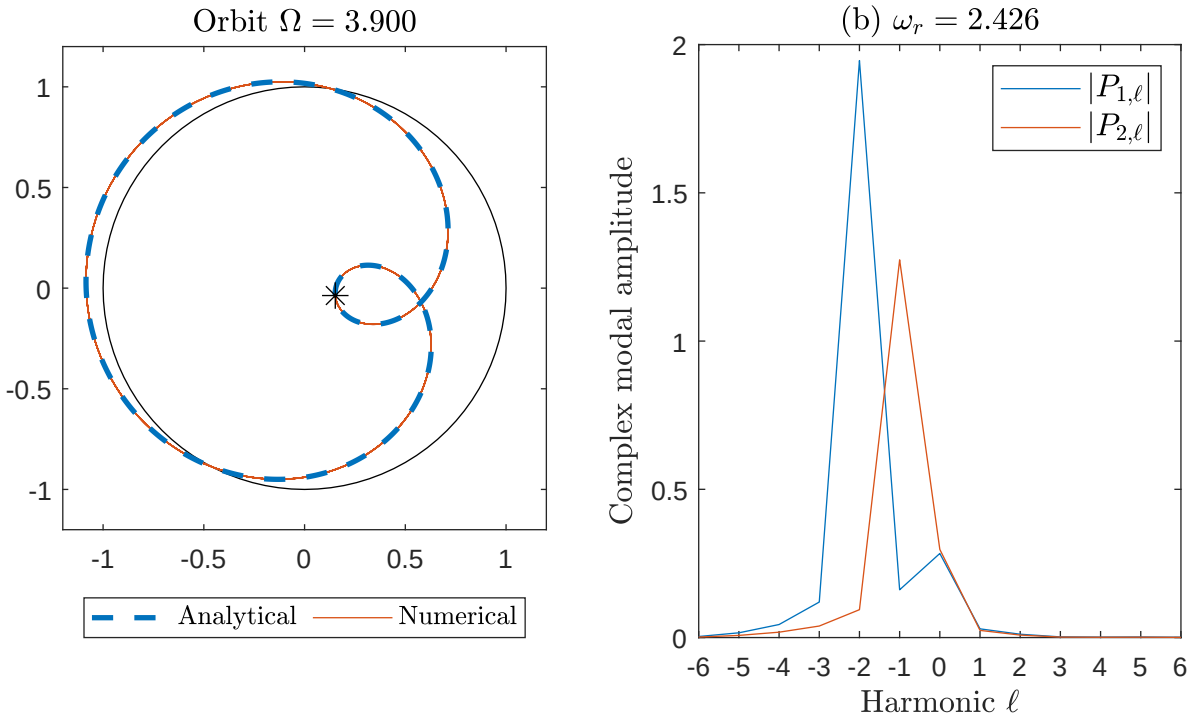

Figure 5: (a) Comparison between analysis and time simulation for a predicted contacting cycle at $\hat{\Omega} = 3.9$, upper solution branch. Thin circle indicates boundary of stator contact, asterisk indicates start/end of period. (b) Amplitude of Fourier components of motion for each complex modal variable.

In order to validate these solutions, the results can be compared to time simulation. The time simulation using the Matlab® [47] function `ode45` with event handling used to accurately locate transition from contact to non contact.

A typical result of this is shown in Fig. 5 (a), which shows the orbit of a the solution for $\hat{\Omega} = 3.9$ taken from the upper solution branch in Fig. 4. It is clear how closely the time simulation tracks the analytical solution. Figure 5 (b) shows the amplitudes of Fourier components of each complex modal variable, taken from the **P** matrix. This confirms our assumption that the resonant terms dominate, the first modal variable at the -2nd harmonic, and the second modal variable at the -1st harmonic, and these are the terms we have captured within **U**. Note there are some other small but visible contributions (which are captured within **H**), most significant of which is the 0th harmonic, which gives the synchronous whirling components. However, away from these and the resonant components the amplitudes of all harmonics rapidly become negligible.

A similar presentation is given in Fig. 6, however in this case the analytical solution is taken from the lower branch of solutions in Fig. 4. The analytical orbit shown in part (a) is similar in character to that shown in Fig. 5 (a), however the 'loop' in the orbit is oriented differently. Furthermore, as shown in part (b), the frequency content and fundamental response frequency ω_r are both quite similar. However, the comparison to time simulation in Fig. 6 (a) shows an apparently poor agreement - in fact the time simulation fails to show a periodic orbit. However, if we follow the time simulation closely from the start (as shown by the asterisk) it can be seen that initially it does follow the analytical solution closely- however, after a few cycles it begins to diverge. This suggests that the analytical and numerical solutions are in agreement, but that this branch of solutions are dynamically unstable. This suggests the existence of a cyclic fold bifurcation for $\hat{\Omega} \approx 3.38$ at which a stable bouncing orbit and an unstable one are created for higher $\hat{\Omega}$-values. Note that a formal stability analysis of these solutions not yet been performed and will be the subject of future work.

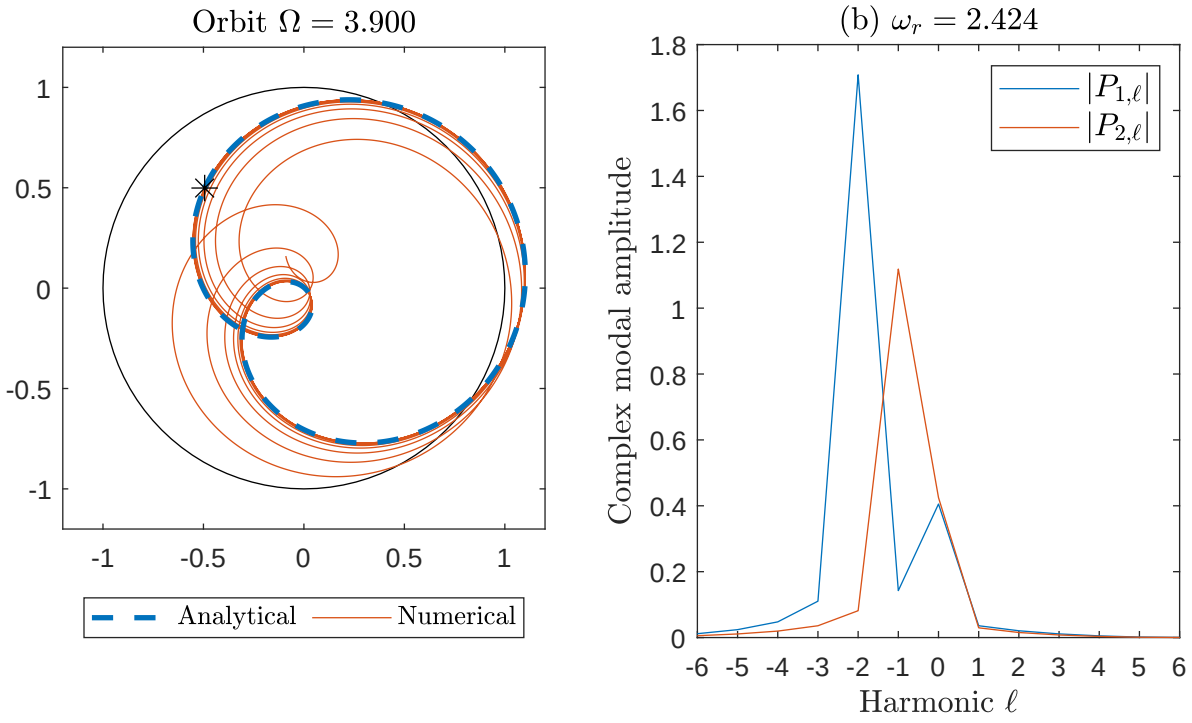

Figure 6: (a) Comparison between analysis and time simulation (30 orbit periods) for a predicted contacting cycle at $\hat{\Omega} = 3.9$, lower solution branch. Thin circle indicates boundary of stator contact, asterisk indicates start/end of period. (b) Amplitude of Fourier components of motion for each complex modal variable.

3.5.2. 3:2 resonance

It was found that the same system, but with twice the out of balance forcing ($\hat{f} = 0.130$), could exhibit a stable 3:2 resonant response. Again, the onset of these solutions is just beyond the value of $\hat{\Omega} = 5.8$, which Figure 3 (b) shows to be the nonlinear critical speed for this internal resonance. Initial guesses in a similar form to (44) were used, however a larger amplitude was required to find solutions:

$$\begin{gathered} U_{1,-3} = 2.5 \\ U_{2,-2} = -2.5,\ -2.5\jmath,\ 2.5,\ 2.5\jmath \\ \text{all other } U_{k,\ell} = 0, \text{ as these are not resonant,} \end{gathered} \tag{45}$$

Numerous 3:2 resonances were found as shown in Figure 7. The previous pattern, where 'upper' branches seem stable and the lower branches are unstable is continued, as shown by figures 8 and 9 respectively which show a stable and an unstable orbit coexisting at the same drive speed.

4. Example 2 - A multi disc rotor

4.1. System description

The method can in principle scale to any number of degrees of freedom in the rotor. An arbitrarily designed rotor with four discs shown in Figure 10, which was chosen as a more challenging test case for analysis with more degrees of freedom.

The shaft is a hollow tube with inner diameter of 3mm, outer diameter 5mm, length 500mm and made from steel assumed to have Young's modulus 210GPa, Poisson ratio 0.3 and density 7810kg/m^3. The shaft is simply supported at each end. There is an inertialess stator at the midpoint of the shaft, with a clearance of 1mm and a contact stiffness of 10N/mm. Hence

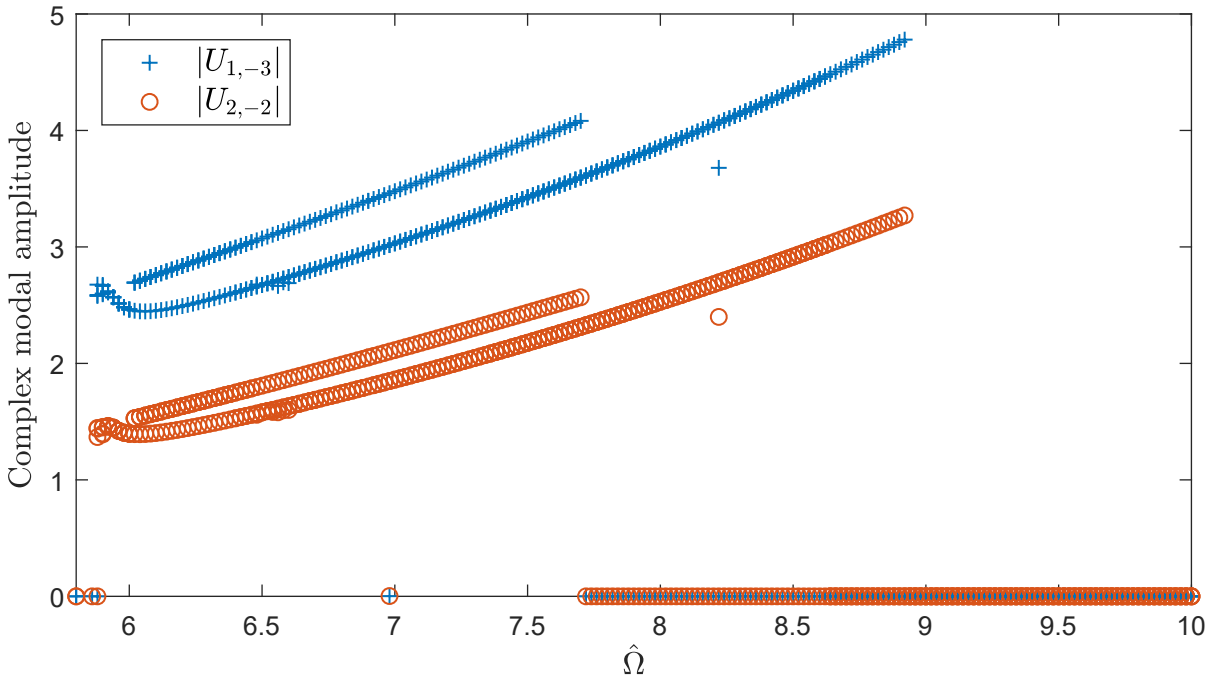

Figure 7: Complex modal amplitudes of resonant components of responses with 3:2 internal resonance at various drive speeds.

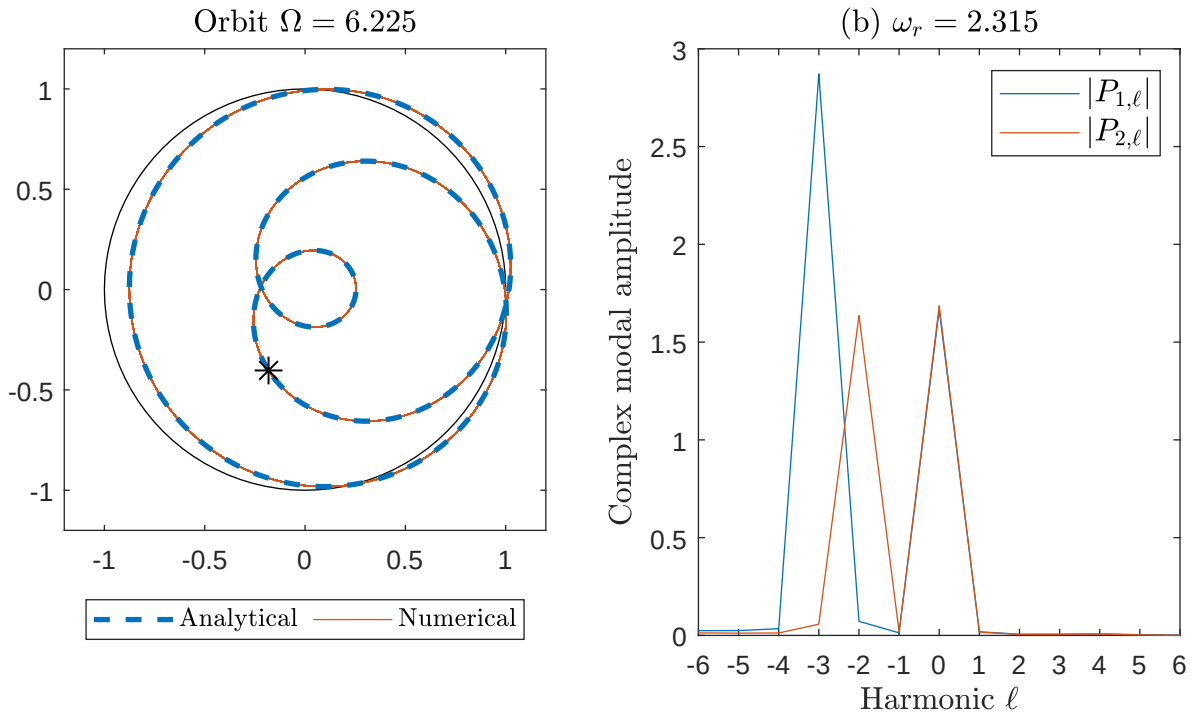

Figure 8: A stable 3:2 orbit, from the higher amplitude solution in Figure 7.

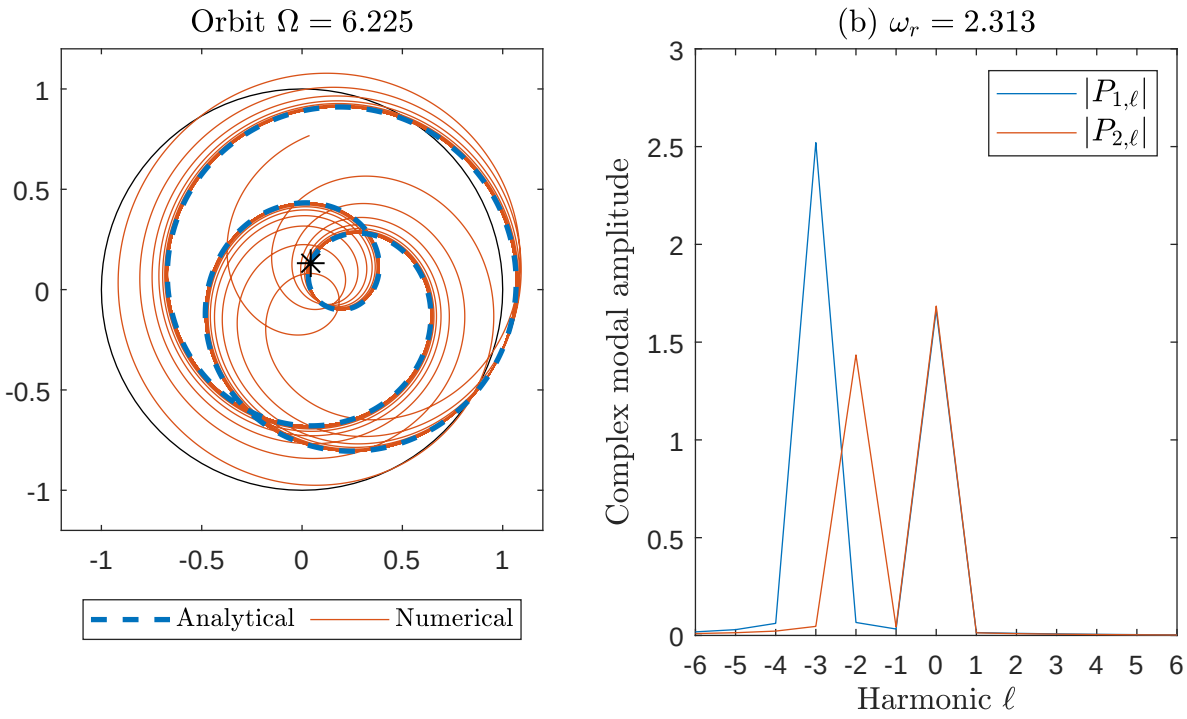

Figure 9: An unstable 3:2 orbit, from the lower amplitude solution in Figure 7.

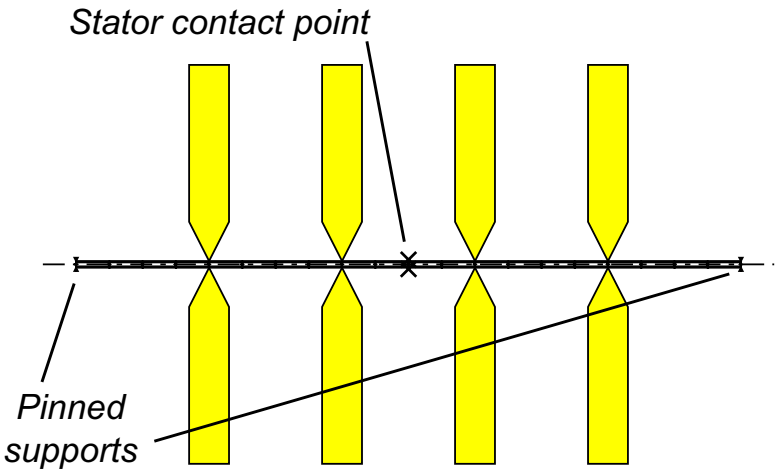

Figure 10: Schematic of multi disc rotor

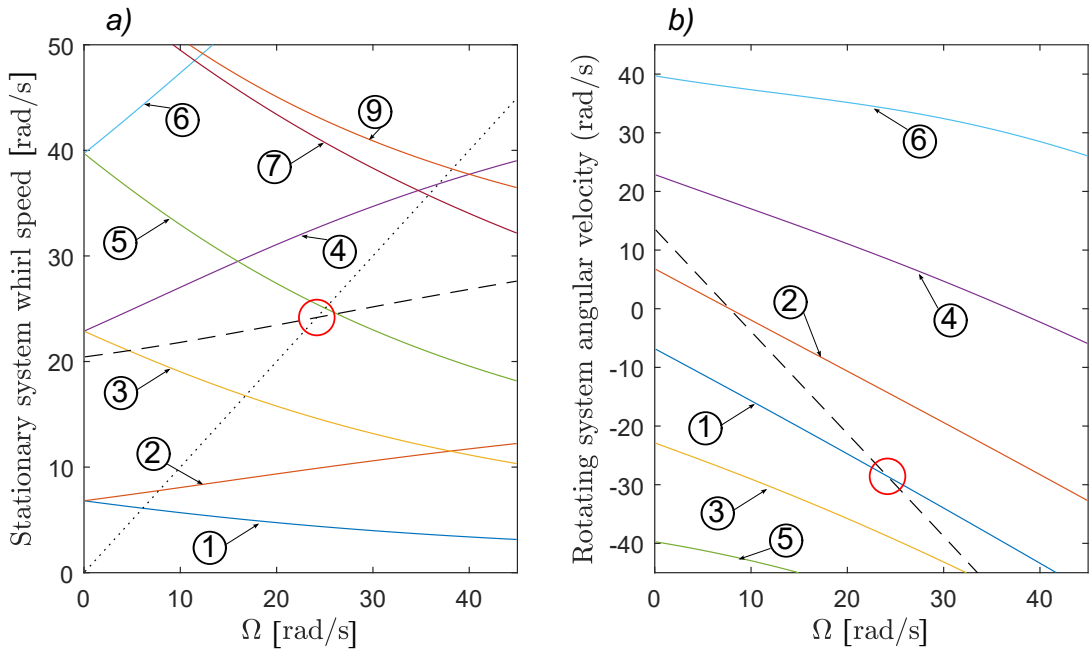

Figure 11: Campbell diagrams for multi disc system, based on underlying conservative system. (a) Stationary system whirl speeds, dotted line shows drive speed Ω, dashed line shows $2\omega_{n2} - \omega_{n1}$. (b) Rotating system whirl velocities, dashed line shows $2\hat{\omega}_{n2}$. Circled numbers indicate each mode's position in the ordering scheme used. Red circles highlight the nonlinear critical speeds for 2:1 internal resonance between modes 1 and 2.

the nonlinear force at this point is given by:

$$\mathbf{f}(\mathbf{x}) = \begin{cases} (k_s(r-1))\,\mathbf{x}/r & , \text{ if } r \geq 0.001 \\ \mathbf{0} & , \text{ if } r < 0.001 \end{cases} \tag{46}$$

where $\mathbf{x}$ is the lateral displacement of the midpoint of the shaft and $r = |\mathbf{x}|$. The four discs are 30mm thick and 300mm in diameter and also made from steel, placed at 100mm intervals along the shaft. An out-of-balance force is added to the 2nd disc from the left, equivalent to this disc being 0.75mm off centre. No gravitational force is present.

4.2. Modelling and solution

The rotor is modelled with a 20 element shaft-line FEA model implemented via the Matlab® based software that accompanies the book [44]. This represents each shaft section as Timoshenko beam, and the discs as lumped mass and inertias. The software outputs stationary coordinate frame mass, gyroscopic, damping and stiffness matrices and an out of balance force vector, that may readily be transformed to the rotating coordinate system, for example by following the process in [33].

The first stage in the analysis is the modal transformation. Unlike the previous example, there are a high number of modes, so a sensible way of sorting the modes must be found. The modes are numbered based upon their stationary coordinate system behaviour, where the first mode is the first backward whirl, the second is the first forward whirl, the third is the second backward whirl, the fourth is the first forward whirl, and so on. This order groups modes with similar shapes together, while avoiding awkward problems with modes apparently crossing as seen in the stationary system Campbell diagram in Figure 11 (a).

It is now necessary to determine the nonlinear critical speeds. By inspecting Figure 11 (b), it can be seen that a drive speed of approximately 24.2rad/s gives $\tilde{\omega}_{n1} = 2\tilde{\omega}_{n2}$, so bouncing solutions might be expected at drive speeds slightly above this value. (The nonlinear critical speed can also be found in the stationary frame condition can be found by using (6) to

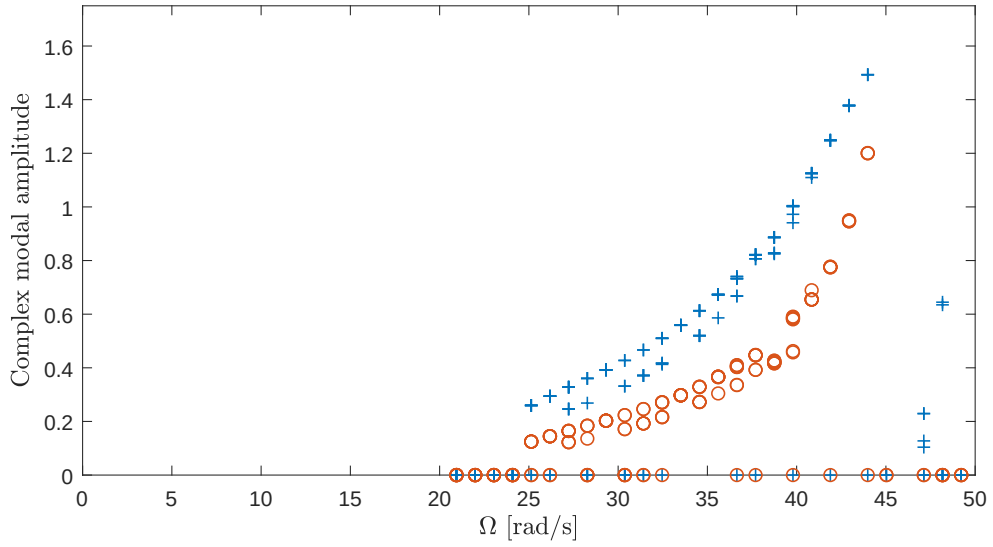

Figure 12: Absolute value of resonant complex components from Normal Forms solution

obtain $\Omega = 2\omega_{n2} - \omega_{n1}$ as discussed in [33], and this is also indicated in Figure 11 (a).) The type of internal resonance is formalised in the method by using the ordered lists $S_k = 1, 2$ and $S_\ell = -2, -1$ similarly to the previous case. Note that S_k could now refer to a far greater range of modes than just the two considered previously.

The initial guesses for $\mathbf{U}$ are again chosen to ensure a response amplitude that gives some penetration into the stator, and also to give a range of phases for $U_{2,-1}$. The list of initial guesses was taken as all permutations of the following lists giving a total of 8 initial guesses:

$$\begin{gathered} a = 0.3, 0.6\ , \\ U_{1,-2} = a\ , \\ U_{2,-1} = a(1+\jmath),\ a(1-\jmath),\ a(-1+\jmath),\ a(-1-\jmath)\ , \\ \text{all other } U_{k,\ell} = 0, \text{ as these are not resonant.} \end{gathered} \tag{47}$$

The initial guess for $\mathbf{H_{-1}}$ is again taken from the underlying linear system's response to the out of balance force.

The simple rotor studied in Section 3 had only two modes and could therefore be solved to an arbitrary degree of precision by choosing a high n_f and converging to a low tolerance. However, when higher modes are present, equation (21) can encounter problems when the value $\Psi_{\ell,\ell} = \ell\jmath\omega_r$ coincides with the kth linear natural frequency held in $\Lambda_{k,k}$. This situation causes the $H_{k,\ell}$ to become large, and usually prevents the solution from converging. These spikes in higher modes have not been seen in simulation, perhaps because in the presence of highly nonlinear responses, the other modal responses no longer act in the same manner. Since these spikes are therefore just an unwanted artefact of the solution method, they must be prevented by truncating the response in terms of frequency, at the cost of some accuracy in the solution. This is done by zeroing all components in $\mathbf{H}$ that are outside the frequency range of the resonant components in $\mathbf{U}$. Furthermore, only the first eight modes of the system are included in the analysis. In the solutions presented, the initial solution is followed by 3 more iterations to improve the accuracy of $\mathbf{H}$.

4.3. Results

Figure 12 shows the results of this analysis over a range of drivespeeds, in terms of the amplitudes of the resonant components. Again, there appear to be corresponding low-amplitude and high-amplitude pairs of solutions. These solution

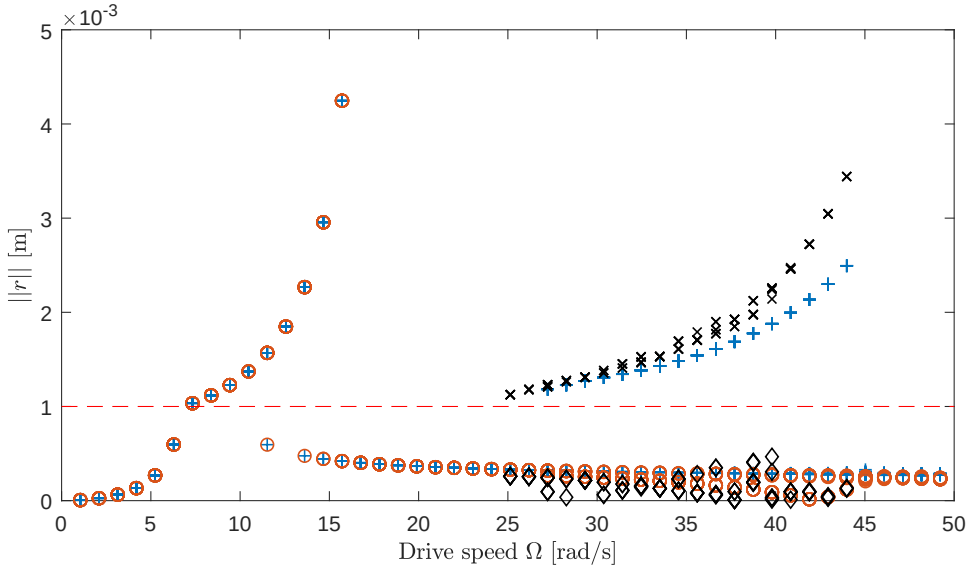

Figure 13: Normal forms results compared to brute force bifurcation. + show max r from simulation, ∘ shows minimum results. Crosses × show the maximum r from analysis, diamonds show the minimum r from analysis. (Non-contacting results from analysis are omitted)

begin at a drive speed of 25rad/s, slightly above the nonlinear critical speed found earlier, as seen in previous cases. A few stray solutions are seen at around 47rad/s; these are very high amplitude solutions that are not connected to the main branch of solutions shown (their equivalent $U_{2,-1}$ points are out of the graph range) and we have not investigated these further.

In an alternative presentation in Figure 13, the analytical results are compared to results from a brute force numerical bifurcation study of this system, following the procedure in [33]. As may be seen, the analytical and numerical solutions accurately show similar maximal drive speeds at which bouncing limit cycles occur,however the lower end of this region is not shown simulation, as these solutions appear to be unstable. The maximum amplitude of displacement is over-predicted by analysis, perhaps because much of the dissipation in a multi rotor system is through higher modes that are truncated in the analysis.

An individual solution is considered in Figure 14 (a). The predicted orbit is again a doubled loop. A time simulation is initiated on the same starting point as the analytical solution, and this matches well although it can be seen that it deviates slightly,reflecting that there is now some more approximation due to truncating the harmonics in the response. Figure 14 (b) shows the amplitude of Fourier components for this response, and it shows that the response is dominated by the resonant components and some synchronous terms; all other components are relatively small. Figure 15 shows the unstable solution at the same drive speed, as shown by the time trace diverging from the analytically predicted orbit after an initial period of approximate agreement. In fact the response is rapidly attracted to the stable response previously shown in Figure 14.

4.4. Encountering additional resonances

A complication occurs in the region of Ω =36.8rad/s; at this speed the 2nd forward whirl (mode 4) becomes critical in the classical linear sense of being directly excited by the out-of-balance forcing, near its resonant frequency. This can be seen in Figure 11 (a) where the line for ω_{n4} intersects the drive speed line; alternatively Figure 11 (b) shows $\tilde{\omega}_{n4}$ passing through zero.

The detailed view of an orbit in this region given in Figure 16 (b) shows that there is indeed a large synchronous spike due to this effect predicted by analysis, although it is seen in Figure 16 (a) that the predicted orbit is still sufficiently near the true solution so that the time simulation stays fairly near. It should be noted the denominator in equation (21) contains

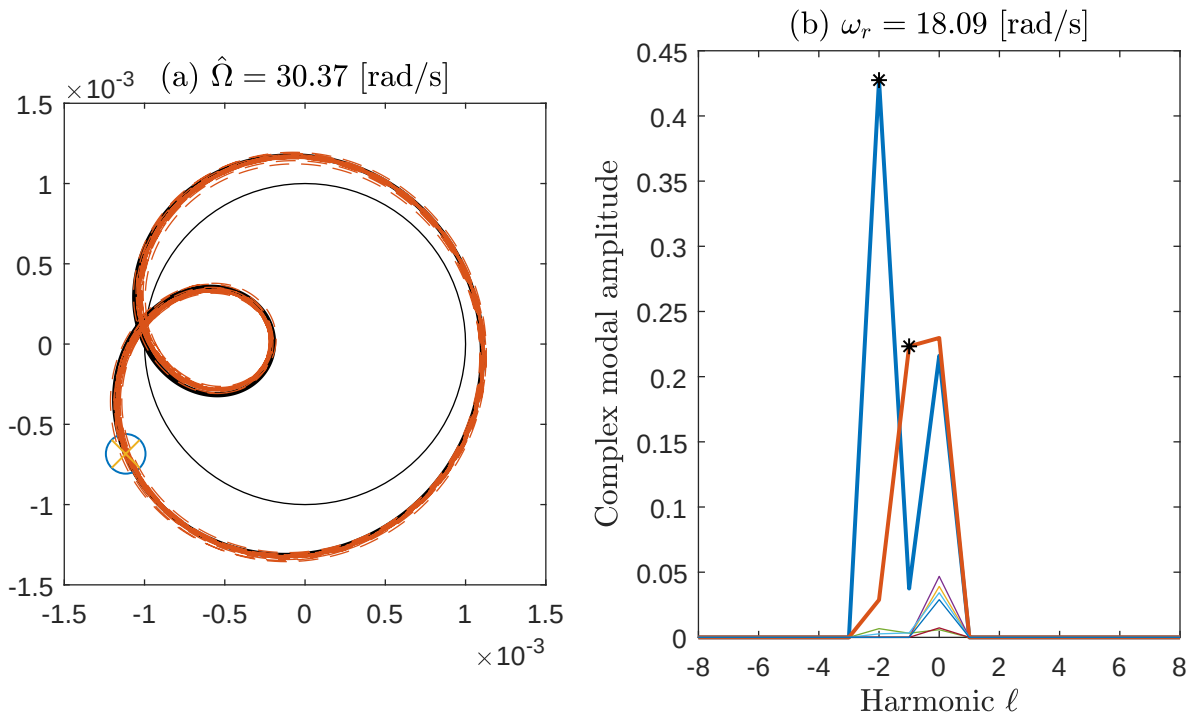

Figure 14: A stable orbit at Ω=30.4rad/s, showing trace of the shaft centrepoint. (a) Solid black line (obscured) shows orbit predicted by normal forms analysis, orange dashed line shows time simulation. Marker shows initial point for both orbits. (b) Amplitude of complex modal components of analytical solution; thick lines show resonant modes and asterisk markers show resonant harmonics of those modes.

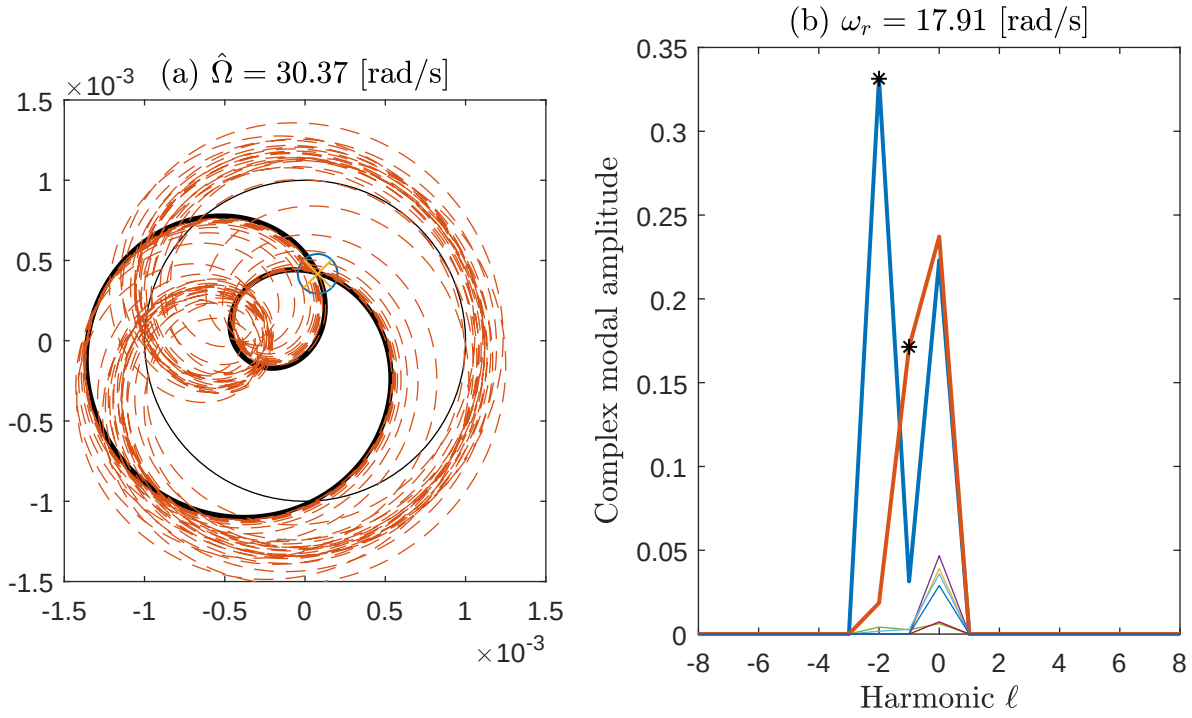

Figure 15: An unstable orbit at Ω=30.4rad/s. (a) Solid black line shows orbit predicted by normal forms analysis, orange dashed line shows time simulation. Marker shows initial point for both orbits. (b) Amplitude of complex modal components of analytical solution; thick lines show resonant modes and asterisk markers show resonant harmonics of those modes.

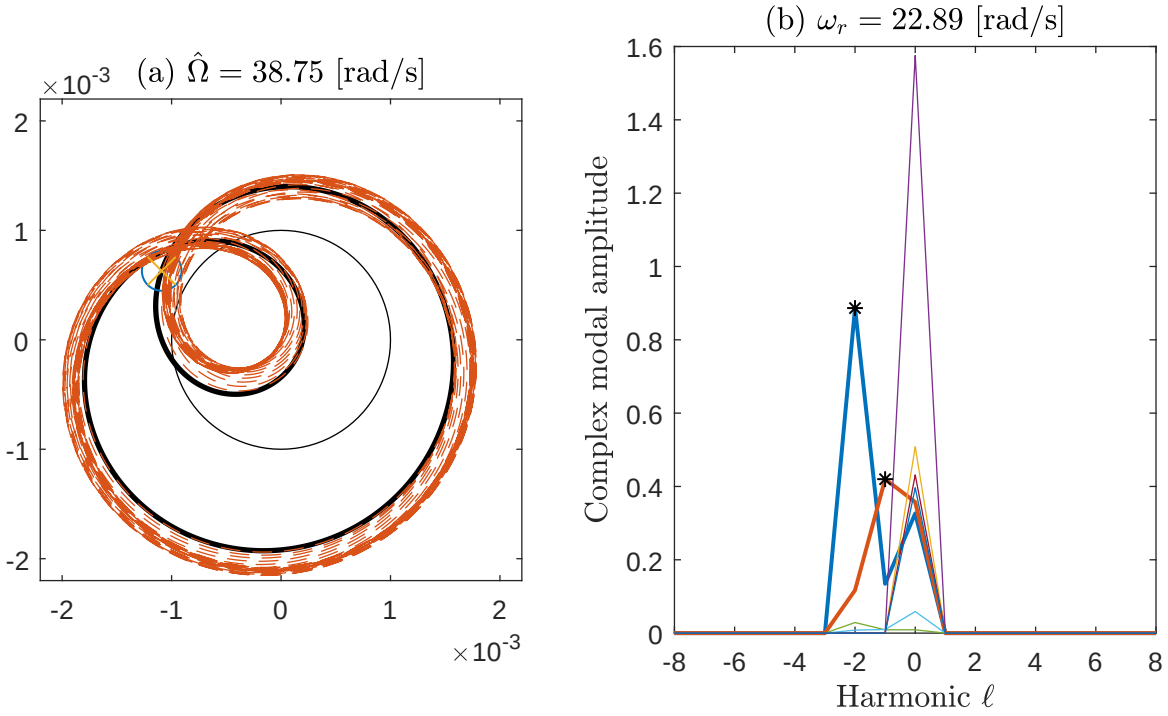

Figure 16: A stable orbit at Ω=38.8rad/s. (a) Solid black line shows orbit predicted by normal forms analysis, orange dashed line shows time simulation. Marker shows initial point for both orbits. (b) Amplitude of complex modal components of analytical solution; thick lines show resonant modes and asterisk markers show resonant harmonics of those modes.

no damping terms, and as such can potentially give infinite results. Figure 17 gives the equivalent to Figure 16 (b), but extracted from a time simulation. This shows that the large synchronous contribution does not appear in reality. The way to handle this more accurately is to include this component as a resonant term, by choosing $S_k = 1, 2, 4$ and $S_\ell = -2, -1, 0$. This results in three resonant harmonic balance equations which can be given explicitly as:

$$\begin{aligned} U_{1,-2}\Psi_{-2,-2} - \Lambda_{1,1}U_{1,-2} - N_{u(1,-2)} = 0 &= -2\jmath\omega_r U_{1,-2} - \jmath\tilde{\omega}_{n1}U_{1,-2} - N_{u(1,-2)} \\ U_{2,-1}\Psi_{-1,-1} - \Lambda_{2,2}U_{2,-1} - N_{u(2,-1)} = 0 &= -\jmath\omega_r U_{2,-1} - \jmath\tilde{\omega}_{n2}U_{2,-1} - N_{u(2,-1)} \\ U_{4,0}\Psi_{0,0} - \Lambda_{4,4}U_{4,0} - N_{u(4,0)} = 0 &= -\jmath\tilde{\omega}_{n4}U_{4,0} - N_{u(4,0)} \end{aligned} \tag{48}$$

noting that $\Psi_{0,0} = 0\jmath\omega_r = 0$. Figure 18 shows a solution of these equations at shaft speed 38.8rad/s, found with the same initial guess as before but with $U_{4,0}$ taken from the damped linear whirl solution. As can be seen the unwanted spike is gone from the solution which is now more similar to that of Figure 17, although the overall accuracy of the orbit seems unimproved. This is perhaps because in this case the 2nd forward whirl mode shape contributes very little at the point where nonlinearity is applied.

5. Conclusions

This work has presented a method for analysing limit cycles in isotropic rotor systems with stator clearances. The method has been built upon the insight that these limit cycles are periodic in a rotating frame, and are a form of internal resonance. The method is very general in both the number of degrees of freedom and the nonlinearities that may be considered, so it is thought that this can be an important step towards more efficient analysis and better understanding of the effects of nonlinearity in complex rotor systems.

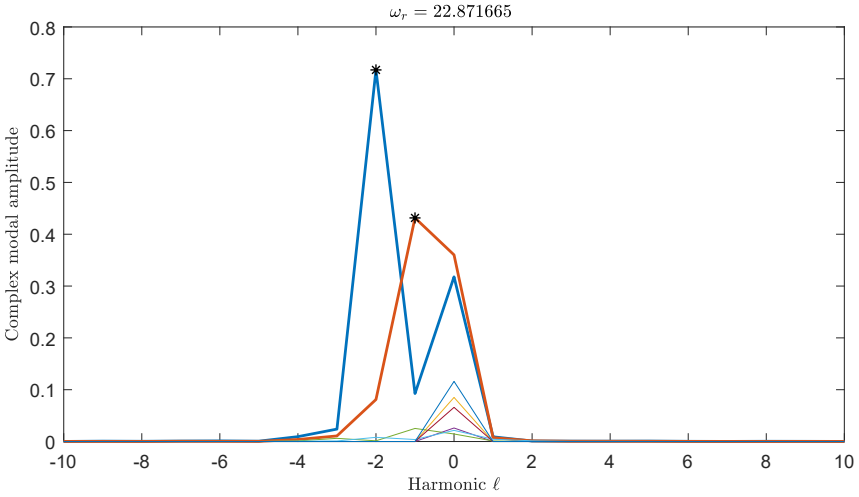

Figure 17: Amplitude of complex Fourier components for 8 modes, extracted from simulation at Ω=38.8rad/s. Bold lines show resonant modes, asterisks show resonant harmonics for those modes.

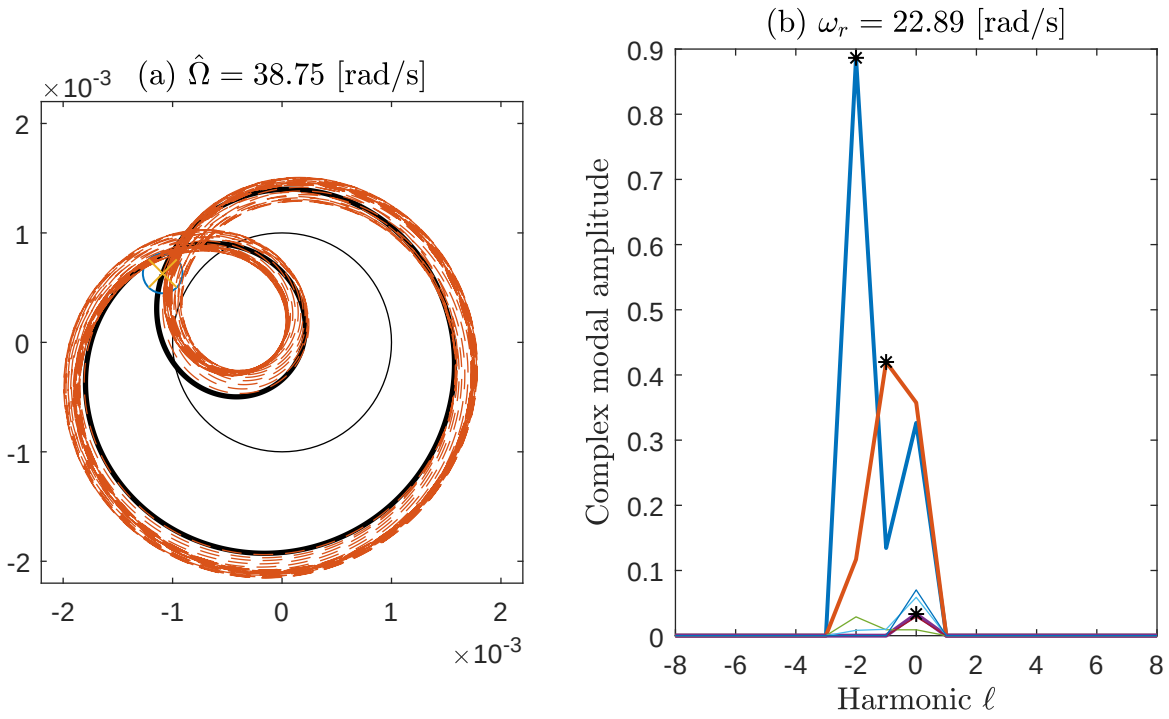

Figure 18: A stable orbit at Ω=38.8rad/s, calculated with three resonant equations as given in (48). (a) Solid black line shows orbit predicted by normal forms analysis, orange dashed line shows time simulation. Marker shows initial point for both orbits. (b) Amplitude of complex modal components of analytical solution; thick lines show resonant modes and asterisk markers show resonant harmonics of those modes.

It has been demonstrated that solutions for a simple overhung rotor can be found with arbitrary precision. This is because while the method primarily solves just for resonant components of the response, it also produces an approximate response for all non-resonant components as well, which may be used repeatedly to refine the result in an iterative scheme. This is much more efficient than solving the full (unreduced) system in one step. The method also gives good approximate results for a multi-disc rotor, although here the accuracy is restricted by the need to truncate harmonics from the response. Work to experimentally validate these findings and extend them to a wider range of systems is underway; it is of keen interest to understand the full robustness of the method in the presence of different forms of nonlinearity and features such as densely spaced modes.

Another pressing question is to predict analytically the presence of these bouncing orbits at drives speeds just beyond the nonlinear critical speeds. The results here suggest that there is a cyclic fold bifurcation. Preliminary investigations, to be reported elsewhere, suggest that this fold bifurcation only reaches the nonlinear critical speed for the internal resonance in the limit that the stator stiffness tends to infinity (the impact limit) and the non-contact damping tends to zero.

Other things that require further investigation include what happens at the high-Ω end of each of these branches of bouncing orbits. From a practical point of view, it is also pressing to establish the basins of attraction of the bouncing orbits, what transient events may trigger them, and what control actions might prevent or alleviate them.

References

[1] G. Jacquet-Richardet, M. Torkhani, P. Cartraud, F. Thouverez, T. N. Baranger, M. Herran, C. Gibert, S. Baguet, P. Almeida, L. Peletan, Rotor to stator contacts in turbomachines. review and application, Mechanical Systems and Signal Processing 40 (2) (2013) 401 – 420. doi:http://dx.doi.org/10.1016/j.ymssp.2013.05.010.
URL http://www.sciencedirect.com/science/article/pii/S0888327013002331

[2] J. Jansen, Non-linear rotor dynamics as applied to oilwell drillstring vibrations, Journal of Sound and Vibration 147 (1) (1991) 115 – 135. doi:http://dx.doi.org/10.1016/0022-460X(91)90687-F.
URL http://www.sciencedirect.com/science/article/pii/0022460X9190687F

[3] S. Ahmad, Rotor casing contact phenomenon in rotor dynamics – literature survey, Journal of Vibration and Control 16 (9) (2010) 1369–1377.

[4] A. Chiba, T. Fukao, O. Ichikawa, M. Oshima, M. Takemoto, D. G. Dorrell, Magnetic bearings and bearingless drives, Elsevier, 2005.

[5] H. Bleuler, M. Cole, P. Keogh, R. Larsonneur, E. Maslen, Y. Okada, G. Schweitzer, A. Traxler, G. Schweitzer, E. H. Maslen, et al., Magnetic bearings: theory, design, and application to rotating machinery, Springer Science & Business Media, 2009.

[6] G. Schweitzer, Safety and reliability aspects for active magnetic bearing applications-a survey, Proceedings of the Institution of Mechanical Engineers, Part I: Journal of Systems and Control Engineering 219 (6) (2005) 383–392.

[7] F. F. Ehrich, Observations of nonlinear phenomena in rotordynamics, Journal of System Design and Dynamics 2 (3) (2008) 641–651.

[8] F. F. Ehrich, Sum and difference frequencies in vibration of high speed rotating machinery, Journal of Engineering for Industry 94 (1) (1972) 181–184.

[9] F. F. Ehrich, J. OConnor, Stator whirl with rotors in bearing clearance, Journal of Engineering for Industry 89 (3) (1967) 381–389.

[10] R. Neilson, A. Barr, Dynamics of a rigid rotor mounted on discontinuously non-linear elastic supports, Proceedings of the Institution of Mechanical Engineers, Part C: Journal of Mechanical Engineering Science 202 (5) (1988) 369–376.

[11] S. Saadat, J. Salichs, M. Noori, Z. Hou, H. Davoodi, I. Bar-On, Y. Suzuki, A. Masuda, An overview of vibration and seismic applications of niti shape memory alloy, Smart Materials and Structures 11 (2) (2002) 218.

[12] U. Ehehalt, O. Alber, R. Markert, G. Wegener, Experimental observations on rotor-to-stator contact, Journal of Sound and Vibrationdoi:https://doi.org/10.1016/j.jsv.2019.01.008.
URL http://www.sciencedirect.com/science/article/pii/S0022460X19300148

[13] W. Szczygielski, Application of chaos theory to the contacting dynamics of high-speed rotors, Rotating machinery dynamics (1987) 319–326.

[14] F. F. Ehrich, High order subharmonic response of high speed rotors in bearing clearance, Journal of Vibration, Acoustics, Stress, and Reliability in Design 110 (1) (1988) 9–16.

[15] A. Muszynska, P. Goldman, Chaotic responses of unbalanced rotor/bearing/stator systems with looseness or rubs, Chaos, Solitons & Fractals 5 (9) (1995) 1683–1704.

[16] F. Chu, Z. Zhang, Bifurcation and chaos in a rub-impact jeffcott rotor system, Journal of Sound and Vibration 210 (1) (1998) 1–18.

[17] S. Edwards, A. W. Lees, M. I. Friswell, The influence of torsion on rotor/stator contact in rotating machinery, Journal of Sound and Vibration 225 (4) (1999) 767–778.

[18] Y. Ishida, Nonlinear vibrations and chaos in rotordynamics, JSME international journal. Ser. C, Dynamics, control, robotics, design and manufacturing 37 (2) (1994) 237–245.

[19] E. V. Karpenko, M. Wiercigroch, E. E. Pavlovskaia, M. P. Cartmell, Piecewise approximate analytical solutions for a jeffcott rotor with a snubber ring, International Journal of Mechanical Sciences 44 (3) (2002) 475–488.

[20] E. V. Karpenko, M. Wiercigroch, M. P. Cartmell, Regular and chaotic dynamics of a discontinuously nonlinear rotor system, Chaos, Solitons & Fractals 13 (6) (2002) 1231–1242.

[21] E. Pavlovskaia, E. Karpenko, M. Wiercigroch, Non-linear dynamic interactions of a jeffcott rotor with preloaded snubber ring, Journal of Sound and Vibration 276 (1) (2004) 361–379.

[22] E. Karpenko, M. Wiercigroch, E. Pavlovskaia, R. Neilson, Experimental verification of jeffcott rotor model with preloaded snubber ring, Journal of Sound and Vibration 298 (4) (2006) 907–917.

[23] F. Chu, W. Lu, Experimental observation of nonlinear vibrations in a rub-impact rotor system, Journal of Sound and Vibration 283 (3) (2005) 621–643.

[24] M. Torkhani, L. May, P. Voinis, Light, medium and heavy partial rubs during speed transients of rotating machines: numerical simulation and experimental observation, Mechanical Systems and Signal Processing 29 (2012) 45–66.

[25] Y. Ishida, T. Inoue, Nonstationary oscillations of a nonlinear rotor during acceleration through the major critical speed: influence of internal resonance (special issue on nonlinear dynamics), JSME International Journal Series C Mechanical Systems, Machine Elements and Manufacturing 41 (3) (1998) 599–607.

[26] Y. Ishida, T. Inoue, Internal resonance phenomena of the jeffcott rotor with nonlinear spring characteristics, Journal of Vibration and Acoustics 126 (4) (2004) 476–484.

[27] Y. Ishida, T. Inoue, Internal resonance phenomena of an asymmetrical rotating shaft, Modal Analysis 11 (9) (2005) 1173–1193.

[28] T. Inoue, Y. Ishida, Chaotic vibration and internal resonance phenomena in rotor systems, Journal of Vibration and Acoustics 128 (2) (2006) 156–169.

[29] M. Cole, P. Keogh, Asynchronous periodic contact modes for rotor vibration within an annular clearance, Proceedings of the Institution of Mechanical Engineers, Part C: Journal of Mechanical Engineering Science 217 (10) (2003) 1101–1115.

[30] P. Keogh, M. Cole, Rotor vibration with auxiliary bearing contact in magnetic bearing systems part 1: Synchronous dynamics, Proceedings of the Institution of Mechanical Engineers, Part C: Journal of Mechanical Engineering Science 217 (4) (2003) 377–392.

[31] K. Mora, C. Budd, P. Glendinning, P. Keogh, Non-smooth Hopf-type bifurcations arising from impact-friction contact events in rotating machinery, Proc. Roy. Soc. Lond. A 470 (2014) art. no. 20140490.

[32] A. Zilli, R. J. Williams, D. J. Ewins, Nonlinear dynamics of a simplified model of an overhung rotor subjected to intermittent annular rubs, Journal of Engineering for Gas Turbines and Power 137 (6) (2015) 065001.

[33] A. D. Shaw, A. R. Champneys, M. I. Friswell, Asynchronous partial contact motion due to internal resonance in multiple degree-of-freedom rotordynamics, Proc. R. Soc. A 472 (2192) (2016) 20160303.

[34] Y. Kim, S. Noah, Y. Choi, Periodic response of multi-disk rotors with bearing clearances, Journal of sound and vibration 144 (3) (1991) 381–395.

[35] Y.-B. Kim, S. Noah, Quasi-periodic response and stability analysis for a non-linear jeffcott rotor, Journal of Sound and Vibration 190 (2) (1996) 239–253.

[36] G. Von Groll, D. J. Ewins, The harmonic balance method with arc-length continuation in rotor/stator contact problems, Journal of sound and vibration 241 (2) (2001) 223–233.

[37] L. Peletan, S. Baguet, M. Torkhani, G. Jacquet-Richardet, Quasi-periodic harmonic balance method for rubbing self-induced vibrations in rotor–stator dynamics, Nonlinear Dynamics 78 (4) (2014) 2501–2515.

[38] D. J. Wagg, S. A. Neild, Nonlinear Vibration with Control, Springer, Dordrecht, 2009.

[39] S. A. Neild, D. J. Wagg, Applying the method of normal forms to second-order nonlinear vibration problems, Proc. R. Soc. A 467 (2128) (2011) 1141 – 1163.

[40] S. A. Neild, A. R. Champneys, D. J. Wagg, T. L. Hill, A. Cammarano, The use of normal forms for analysing nonlinear mechanical vibrations, Phil. Trans. R. Soc. A 373 (2051) (2015) 20140404.

[41] L. Stolovitch, Progress in normal form theory, Nonlinearity 22 (7) (2009) R77.

[42] M. H. Fredriksson, A. B. Nordmark, On normal form calculations in impact oscillators, Proceedings of the Royal Society of London A: Mathematical, Physical and Engineering Sciences 456 (1994) (2000) 315–329.

[43] T. H. Cameron, J. H. Griffin, An alternating frequency/time domain method for calculating the steady-state response of nonlinear dynamic systems, Journal of applied mechanics 56 (1989) 149.

[44] M. I. Friswell, J. E. T. Penny, S. D. Garvey, A. W. Lees, Dynamics of Rotating Machines, Cambridge, 2010.

[45] A. D. Shaw, A. R. Champneys, M. I. Friswell, Two mode backbone curves for analysis of a rotor-stator contact system, in: International Conference on Noise and Vibration Engineering (ISMA), Leuven, Belgium, 2016.

[46] S. A. Neild, Approximate methods for analysing nonlinear structures, in: L. N. Virgin, D. J. Wagg (Eds.), Exploiting Nonlinear Behaviour in Structural Dynamics, Springer, 2012, pp. 53 – 109.

[47] M. Inc., Matlab and simulink for technical computing (July 2012).
URL `http://www.mathworks.com`